



โครงการ
การเรียนการสอนเพื่อเสริมประสบการณ์

ชื่อโครงการ การศึกษาและสังเคราะห์อนุภาคนาโนจากพอลิเมอร์สายเดี่ยวสำหรับการผลิต
แก๊สไฮโดรเจน

En Route to the Synthesis of Single Chain Nanoparticles for
Hydrogen Evolution

ชื่อนิสิต นายทองพล หมีทอง

ภาควิชา เคมี

ปีการศึกษา 2560

คณะวิทยาศาสตร์ จุฬาลงกรณ์มหาวิทยาลัย

**En Route to the Synthesis of Single Chain Nanoparticles
for Hydrogen Evolution**

การศึกษาและสังเคราะห์อนุภาคนาโนจากพอลิเมอร์สายเดี่ยว
สำหรับการผลิตแก๊สไฮโดรเจน

by

Mr. Thongpon Meethong

**A Report Submitted in Partial Fulfillment of the Requirements
For the degree of Bachelor of Science Program in Chemistry**

Department of Chemistry

Faculty of Science

Chulalongkorn University

Academic year 2017

Title En Route to the Synthesis of Single Chain Nanoparticles for Hydrogen Evolution

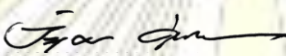
By Mr. Thongpon Meethong

Accepted by the Faculty of Science, Chulalongkorn University in Partial Fulfillment of the Requirement for bachelor's degree

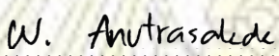
COMMITTEE

 Chairman

(Associate Professor Voravee P. Hoven, Ph.D.)

 Advisor

(Junjuda Unruangsri, D.Phil.)

 Examiner

(Wipark Anutrasakda, Ph.D.)

Report has been approved by Head of the Department of Chemistry

..... Head of the Department of Chemistry

(Associate Professor Vudhicaï Parasuk, Ph.D.)

Date..... May 2018

Quality of report Very Good Good Fair

Acknowledgements

I would like to thank all the following persons for their supports, advices and encouragements during my study.

First of all, I would like to express my sincere gratitude to my advisor Dr. Junjuda Unruangsri for the continuous advices, patience, motivation and knowledge of my senior project. Her guidance always assists me to achieve the experiments and report. I really appreciate to all supports from committee members, Associate Professor Voravee P. Hoven and Dr. Wipark Anutarasakda in every insightful comment.

I would like to thank Dr. Parichatr Vanalabpatana who provides me instruments and useful knowledge about Cyclic Voltammogram.

I would like to thank Dr. Kittipong Chainok for producing crystallographic data and model.

I would like to thank all members of VH group and SCRUI for their kindness and helps in laboratory.

Finally, I am appreciated all of encouragements and supports from my family and friends. Without all of you, I could not imagine how do I pass this tough four years in the university. I would like to thank from the bottom of my heart.



Contents

บทคัดย่อ	Error! Bookmark not defined.
Abstract	Error! Bookmark not defined.
Acknowledgements	c
Contents	f
List of Figures	h
List os Schemes	j
List of Abbreviations	k
Chapter 1: Introduction	1
1.1 Motivation	1
1.2 Catalysts for Hydrogen Evolution	1
1.3 Single Chain Nanoparticles (SCNPs)	4
1.4 Objectives	9
1.5 Expected Result	9
Chapter 2: Results and Discussion	10
2.1 Synthesis of Ferrocene-derivative Compounds	11
2.1.1 The Synthesis of 1,1'-Bis(diphenylphosphenyl)ferrocene (dppf, 1)	11
2.1.2 The Synthesis of (dppf)NiCl ₂ (2)	13
2.1.3 The Synthesis of (dppf)Ni(S ₂ C ₆ H ₄) (3)	14
2.1.4 The Synthesis of (dppf)Ni(SC ₆ H ₅) ₂ (4)	15
2.2 The Study of Redox Behavior of Compound 3 and Its Reactivity Towards Hydrogen Evolution	16
2.3 The Synthesis of Single Chain Nanoparticles (SCNPs)	19
2.3.1 The Synthesis of Poly(pentafluorophenyl Acrylate (poly(PFPA)))	19
2.3.2 The Synthesis of Modified Poly(PFPA)	21
2.3.3 The Synthesis of Single Chain Nanoparticles of Modified Poly(PFPA)	25

Chapter 3: Experimental	29
3.1 Materials and Instruments	29
3.1.1 Materials	29
3.1.2 Instruments	30
3.2 Experimental Procedures	32
3.2.1 Synthesis of ferrocene-derivative compounds	32
3.2.1.1 Synthesis of 1,1'-Bis(diphenylphosphenyl)ferrocene (dppf, 1)	32
3.2.1.2 Synthesis of (dppf)NiCl ₂ (2)	32
3.2.1.3 Synthesis of (dppf)Ni(S ₂ C ₆ H ₄) (3)	33
3.2.1.4. Attempt to Synthesis of (dppf)Ni(SC ₆ H ₅) ₂ (4)	34
3.2.2 Synthesis of Single Chain Nanoparticles (SCNPs)	34
3.2.2.1 Synthesis of pentafluorophenyl acrylate (PFPA)	34
3.2.2.2 Synthesis of poly(pentafluorophenyl acrylate (poly(PFPA)))	34
3.2.2.3 Synthesis of modified poly(PFPA) with 2-aminothiophenol	35
3.2.2.4 Attempt to Synthesis of Single-chain Nanoparticles of poly(PFPA)	35
Chapter 4: Conclusion	36
References	37
Vita	41



List of Figures

- Figure 1.1** Active site structure of [Fe–Fe]-hydrogenase (left) and [Ni–Fe]-hydrogenase (right). 2
- Figure 1.2** Ru-PNN complexes and catalytic process. 2
- Figure 1.3** X-ray crystallography of (dppf)Ni(bdt) (left) and cyclic voltammogram in the presence of varying concentration of CH₃COOH (right). 3
- Figure 1.4** Illustration of metallo-folded SCNPs via intramolecular cross-linking interaction (A) and complexation (B). 5
- Figure 1.5** Illustration of the Pd-SCNP formation via the intramolecular crosslinking. 6
- Figure 1.6** Schematic illustration of the synthesis of the copper-containing MONPs and its internal structure of the cross-linkage. 7
- Figure 1.7** Illustration of the thiol-functionalized linear copolymer P(MMA₃₃₅-*co*-HEMA₇₃-*co*-MPEMA₅₀) and its intramolecular self-folding with metal-thiolate coordination. 8
- Figure 2.1** Illustration of Ni-SCNP via intramolecular crosslinking of modified poly(PFPA) by metal-ligand complexation. 10
- Figure 2.2** ¹H NMR in CD₂Cl₂ of 1,1'-Bis(diphenylphosphenyl)ferrocene (dppf, **1**). 12
- Figure 2.3** Sample solution of (dppf)NiCl₂ for UV-Vis measurement (left) The complementary color circle in different wavelength (right). 13
- Figure 2.4** ¹H NMR (400.0 MHz, CDCl₃, 297 K) of (dppf)Ni(S₂C₆H₄) (**3**). 14
- Figure 2.5** ³¹P{¹H} NMR (376.5 MHz, CDCl₃, 297 K) of **4** at 2 h (A) and 24 h (B). 15
- Figure 2.6** ¹H NMR (400.0 MHz, CDCl₃, 297 K) of (dppf)Ni(SC₆H₅)₂ 16
- Figure 2.7** Cyclic voltammogram of **3** in DMF at a potential scan rate of 100 mV/s. 17
- Figure 2.8** Cyclic voltammograms of **1** in the presence of varying concentration of acetic acid (CH₃COOH). The concentrations are 0, 32, 128 and 512 mM. 18

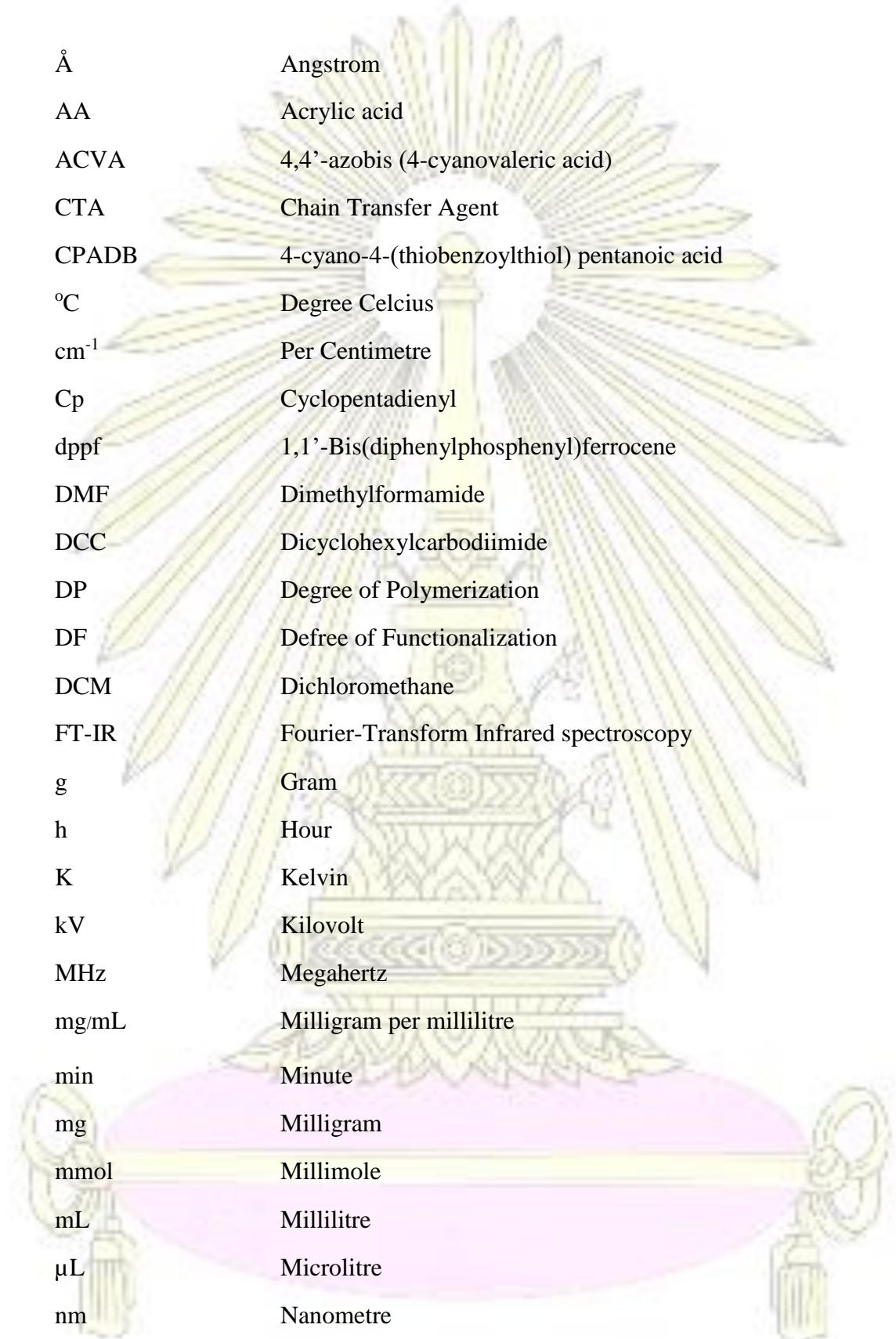
- Figure 2.10** $^{19}\text{F}\{^1\text{H}\}$ NMR (376.5 MHz, CDCl_3 , 297 K) of crude modified poly(PFPA) at 22 h. 22
- Figure 2.11** Possible productd formed in the modification of poly(PFPA) with 2-aminothiophenol. (R is polymeryl group). 23
- Figure 2.12** Stacked IR spectra of poly(PFPA) (blue) and modified poly(PFPA) with 2-aminothiophenol (red). 23
- Figure 2.13** Nucleophilic substitution intermediate of 2-aminothiophenol. 24
- Figure 2.14** UV-Vis spectra at RT of **2** (green) and SCNPs with adding amount of NEt_3 2.4 μL (0.3eq. to $[\text{Ni}^{2+}]$) (black), 4.8 μL (0.6 eq. $[\text{Ni}^{2+}]$) (blue) and 7.2 μL (1.0 eq. $[\text{Ni}^{2+}]$) (red). 25
- Figure 2.15** $^{31}\text{P}\{^1\text{H}\}$ NMR (161.9 MHz, 10% CDCl_3 in THF-H_8 , 298K) of crude SCNPs. 26
- Figure 2.16** TEM micrographs of SCNPs and their aggregation. 27
- Figure 2.17** DLS spectrum of SCNPs. 27
- Figure 2.18** DLS spectrum of aggregated SCNPs. 28

List of Schemes

- Scheme 2.1** The synthetic routes for ferrocene-derivative compounds: dppf (**1**), (dppf)NiCl₂ (**2**), (dppf)Ni(S₂C₆H₄) (**3**) and (dppf)Ni(SC₆H₅)₂ (**4**). 11
- Scheme 2.2** Equilibrium between the possible structure of monomeric nickel thiolate compound and oligomeric Ni-S bridged compound. 16
- Scheme 2.3** The synthesis of PFPA (monomer) and poly(PFPA) via a RAFT polymerization. 19
- Scheme 2.4** The modification of poly(PFPA) with 2-aminothiophenol (**P1**). 21



List of Abbreviations



Å	Angstrom
AA	Acrylic acid
ACVA	4,4'-azobis (4-cyanovaleric acid)
CTA	Chain Transfer Agent
CPADB	4-cyano-4-(thiobenzoylthiol) pentanoic acid
°C	Degree Celcius
cm ⁻¹	Per Centimetre
Cp	Cyclopentadienyl
dppf	1,1'-Bis(diphenylphosphenyl)ferrocene
DMF	Dimethylformamide
DCC	Dicyclohexylcarbodiimide
DP	Degree of Polymerization
DF	Defree of Functionalization
DCM	Dichloromethane
FT-IR	Fourier-Transform Infrared spectroscopy
g	Gram
h	Hour
K	Kelvin
kV	Kilovolt
MHz	Megahertz
mg/mL	Milligram per millilitre
min	Minute
mg	Milligram
mmol	Millimole
mL	Millilitre
µL	Microlitre
nm	Nanometre
NMR	Nuclear Magnetic Resonance Spectroscopy

PFPA	Pentafluorophenyl Acrylate
PFP	Pentafluorophenol
ppm	Parts per million
RT	Room temperature
RAFT	Reversible Addition-Fragmentation Chain-Transfer
SCNPs	Single Chain Nanoparticles
TEM	Transmission Electron Microscopy
TMEDA	N,N,N',N'-tetramethylethylenediamine
THF	Tetrahydrofuran
UV-Vis	UV-Visible spectroscopy
V	Volt



Chapter 1

Introduction

1.1 Motivation

World's population growing rate has been increasing over a century, this brings the energy consumption significantly higher. The need for energy production to serve humans' activities is hence multiplied, of which is in line with an increasing of pollution. The major source of pollutants can be classified into 2 types: non-road engines and vehicles. Firstly, the engines in factories or plants emit the greenhouse gases (GHGs) consisting of water vapor, carbon dioxide, methane and etc., which affect the world's temperature and climate change. In addition, most of vehicles use fossil fuels as a power source for combustion and emit toxic wastes, such as carbon monoxide, nitrogen dioxide, lead and dust particles, which cause global warming and directly affect human's health. To lower these drawbacks from fossil fuel energy, many types of alternative energy were created and developed from natural sources such as sunlight, wave/tidal and wind energy. Unfortunately, energy converting catalysts were limited to produce enough energy for our lives.

Nowadays, hydrogen gas plays a key role as a clean alternative energy source due to its colorless, odorless, non-poisonous and unlimited source.¹⁻² Electrolysis and steam-methane reforming processes are common methods to produce hydrogen gas.³⁻⁴ Nevertheless, the manufacturing processes still emit such air pollutants. Hence, novel technologies for effective production of hydrogen are still needed. The new technology commonly requires inorganic catalysts to gain highest hydrogen gas production derived from proton-containing species. Although extensive studies of the artificial catalysts have been anticipated yet the challenge remains.

1.2 Catalysts for Hydrogen Evolution

A type of biological enzyme for an interconversion of protons to hydrogen is called hydrogenases.⁵ This enzyme can be divided into three sub-classes comprising 5,10-methynyltetrahydromethanopterin hydrogenase (Hmd), [Ni-Fe]-hydrogenases and [Fe-Fe]-hydrogenases. Among the three sub-classes, [Ni-Fe]-hydrogenases and [Fe-Fe]-hydrogenase have received highest interest due to high reversibility and catalytic activities. The conceived properties of these cluster derived from the structural from a dimetal carbonyl/cyano core connected with an azadithiolate bridge (**Figure 1.1**) as an important functional group.

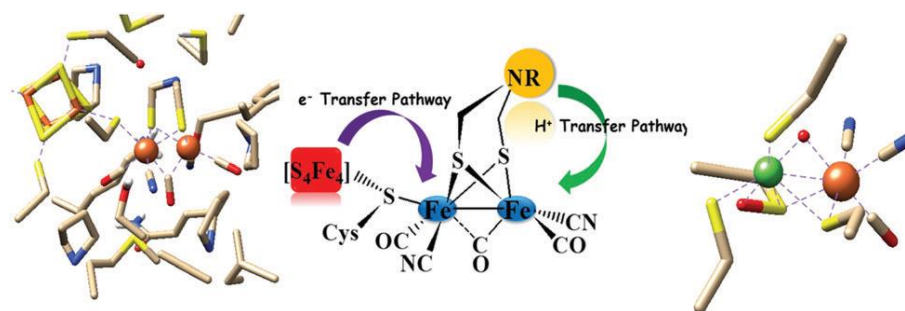


Figure 1.1 Active site structure of [Fe-Fe]-hydrogenase (left) and [Ni-Fe]-hydrogenase (right).⁵

Attempts to produce inorganic catalysts by imitating biological hydrogenase enzyme were carried out as illustrated through the work of Hu *et al.* in 2014.⁶ Monometallic Ru-PNN catalyst was successfully synthesized for hydrogen production from MeOH and water. Ru-PNN catalyst converted MeOH to H₂ and CO₂ at below 100°C with high yield (~80%). **(Figure 1.2)** This catalyst could be reused without purification and catalytic properties can be maintained over a period of one month.

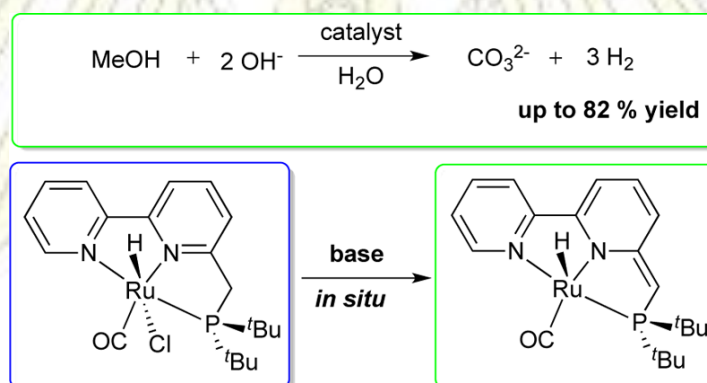


Figure 1.2 Ru-PNN complexes and catalytic process.⁶

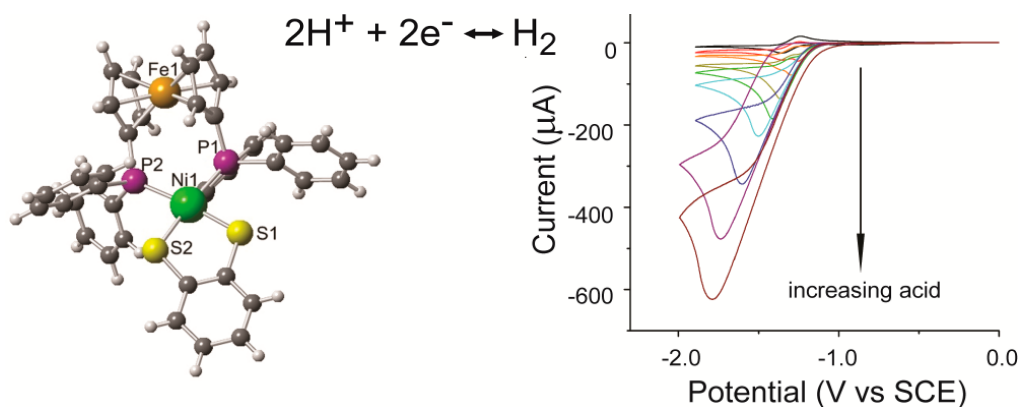


Figure 1.3 X-ray crystallography of (dppf)Ni(bdt) (left) and cyclic voltammogram in the presence of varying concentration of CH_3COOH (right).⁷

In the later year, the bimetallic homogeneous catalyst which is the more resembled to the [Ni-Fe] hydrogenase enzyme was produced by Lu Gan's group.⁷ The complex contained nickel atom which was coordinated with both potentially redox active bdt (1,2-benzenedithiolate) and dppf (bis(diphenylphosphino)ferrocene) ligands. **(Figure1.3)** The complex entails the selective catalytic activity towards the proton reduction for the hydrogen evolution reactions. The complex was stable and efficiently catalyze the hydrogen production with high turnover number and a low over potential. This study inspired the synthesis route and the further applicable modification of bimetallic catalyst.

Although this catalyst showed very high activity for hydrogen production, the major drawback is its solubility in water. Hence, the catalytic activity is impeded with aqueous proton source.

1.3 Single Chain Nanoparticles (SCNPs)

Nanoparticles have been studied in the recent decades.⁸ Generally, nanoparticles have size between 1-100 nm including surrounding interfacial layer. Due to their valuable applications in many fields of sensors and catalysts, scientists have developed the synthetic pathways along with exploring their behaviors and functions. The specific functions rely on their designable sizes, shapes as well as modified surfaces. From these points, the different properties of nanoparticles were brought out; including hydrophilicity, reactivity, electronic structure and stability.

Single chain nanoparticles (SCNPs) are one of the novel nanomaterials with their crucial applications, for example, nanomedicine, image contrast agent, sensor, and catalyst.⁹⁻²⁰ These technologies derived from a single polymeric chain to form a soft-nano object which specifically composed of numerous nano-cavities containing the active or catalytic sites. The folded particles can enhance the physical and chemical properties of previous ordinary nanoparticles, metal nanoparticles or cluster. Discrete polymeric chains were used as the backbone whereby the side-chain functional groups can be modified up to purposes. The interactions facilitating the folding or collapsing of the polymeric backbones are intramolecular cross-linking interactions, covalent bonding between functional groups or coordination interaction with metal ions as shown in **Figure 1.4**. As a result, 3-dimensional nano-object exhibiting advantages can be obtained with cited applications.

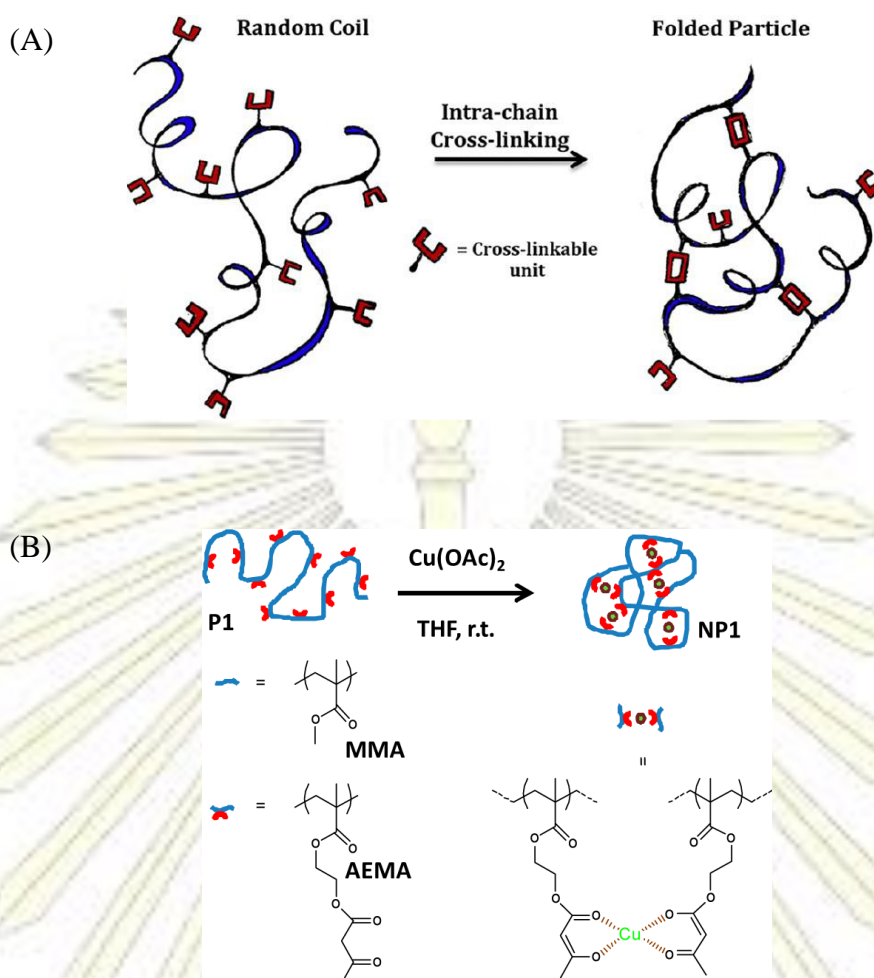


Figure 1.4 Illustration of metallo-folded SCNPs via intramolecular cross-linking interaction (A) and complexation (B).²¹⁻²²

Furthermore, SCNPs could potentially act as an enzyme mimic catalyst.²³⁻²⁵ Due to the importance of enzyme in biology, the scientists have been enthusiastically trying to synthesize an artificial enzyme with a precise active site position and size. Two main parts of SCNPs are polymeric chain and functionalized groups. They can be compared to an amino sequence and catalytic site in a bio-enzyme, respectively. However, the polymeric chain normally provides hydrophobicity which rarely dissolves in water environment. To solve these problems, some hydrophilic functionalized groups were filled in the structure.²⁶ From the above mentioned information, properties of polymer and catalysts can be tuned for specific purposes with an increase of the concentration of active site in nanoparticles and turnover rate. Because of the numerous usage and the lack of a study, we focused on the catalyst application of SCNPs.

SCNPs combine good points of homogeneous and heterogeneous catalysts in one. The catalyst would present hydrophobicity and hydrophilicity in different conditions, so we could easily remove the catalyst from product to use repeatedly as the heterogeneous catalysts. The nanosized polymers make the structure hollow, so the catalytic sites are elevated to be mostly equal to the homogeneous catalysts. The uses of SCNPs as catalysts have been anticipated for the highest product yield and reusability.

The synthesis of SCNPs began with investigation of the appropriate interaction by mimicking natural enzyme to crosslink the polymeric chain into the nanoparticles. In 2015, The research of Meng Huo *et al.*²³ has shed some light on the developing of the synthetic strategies of SCNPs. From the experimental results, they proposed four routes to produce SCNPs, namely, the coupling of two functional groups on polymeric chain via covalent bonding, non-covalent crosslinking (π - π and supramolecular interaction), dynamic covalent crosslinking (disulfide, imine and acylhydrazone bonds) and protein mimicry. They made SCNPs performs like enzyme due to increasing dynamic adaptivity. All strategies can be proved the formation of SCNPs by size-exclusion chromatography (SEC).

In the same year, Willenbacher *et al.* presented the novel SCNPs catalyst using the copolymerization of polystyrene and 4-(chloromethyl)styrene (CMS) as the polymer template.²⁷ The post-polymerization modification was carried out with triarylphosphine. (Pd[1,5-cyclooctadiene]Cl₂) was used as a precursor to obtained the Pd-SCNPs used as a catalyst in the Sonogashira coupling reaction of 2-bromopyridine and phenylacetylene (**Figure1.5**). Therefore, this study could ensure the fabrication of SCNPs by the acceptable modification process and showed the potential use of SCNPs in organic transformation.

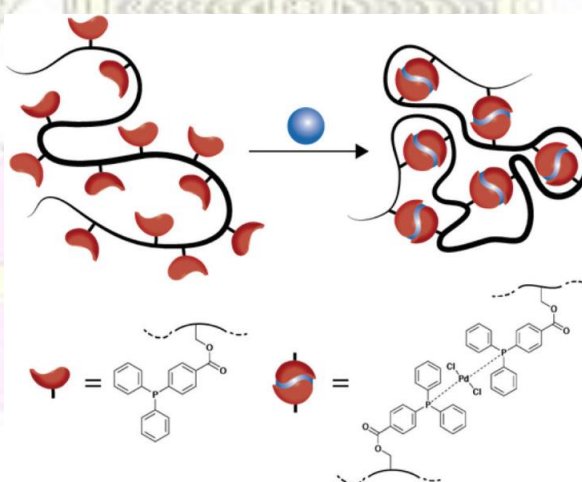


Figure 1.5 Illustration of the Pd-SCNP formation via the intramolecular crosslinking.²⁷

The enzyme mimic nanoparticles could be used in a well-known organic reaction. Bai *et al.* suggested the copper-containing metal-organic nanoparticles (MONPs) for catalysis the alkyne-azide “click chemistry” reaction in water (**Figure 1.6**).²⁸ N-butylimidazole was added to polymer which provide more solubility in water. To form the nanoparticle, the aspartate-functionalized group will form a coordination complex with Cu^{2+} . The obtained metal-organic nanoparticles can successfully catalyze alkyne-azide “click” reaction with phenylacetylene and benzyl azide. Moreover, this material entailed high yield of product. Hence, the synthesis route and catalytic performance inspired high possibility of beneficial SCNPs in an aqueous environment.

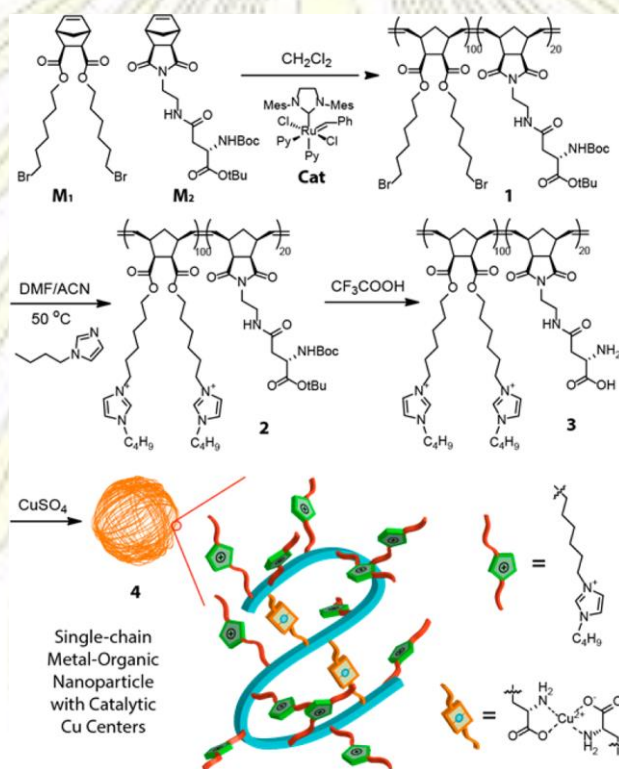


Figure 1.6 Schematic illustration of the synthesis of the copper-containing MONPs and its internal structure of the cross-linkage.²⁸

Recently, SCNPs have been used as catalyst to capture and convert CO₂ to carbon-based fuel. In 2017, Srinivas *et al.* reported the novel artificial nano-catalyst for photocatalytic reduction of CO₂.²⁹ They initially fabricated the thiol-functionalized linear copolymer, poly(methylmethacrylate-*co*-hydroxyethylmethacrylate-*co*-2-(3-mercaptopropanoyloxy)ethyl methacrylate (P(MMA₃₃₅-*co*-HEMA₇₃-*co*-MPEMA₅₀)), by post-polymerization. Nickel-thiolate bonding folded the polymeric chain into nanoparticles as shown in **Figure 1.7**. This nano-catalyst worked effectively in the presence of light, called photocatalyst with TiO₂ as photosensitizer and triethanolamine as an electron donor. The result shows the effectiveness of the CO₂ conversion which can achieve at high temperature. Thus, the novel artificial nano catalyst from discrete polymeric chain for CO₂ reduction can be obtained.

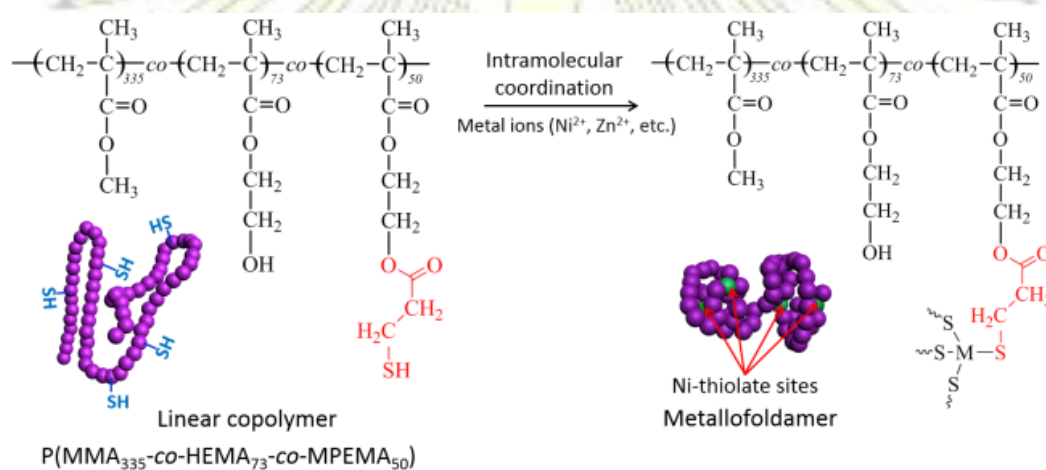


Figure 1.7 Illustration of the thiol-functionalized linear copolymer P(MMA₃₃₅-*co*-HEMA₇₃-*co*-MPEMA₅₀) and its intramolecular self-folding with metal-thiolate coordination.²⁹

In this project, we focused on the synthesis of SCNPs mimicking [Ni-Fe] functional group of hydrogenase enzyme to solve the water solubility problem from the mentioned previous catalysts. Along with the SCNPs, the homogeneous analogues were synthesized to investigate their structural properties and catalytic activity in hydrogen production. Characterization of the gained SCNPs will be performed by NMR spectroscopy, UV-Visible spectroscopy, ATR-IR spectroscopy, X-ray Crystallography, Elemental analysis, Electrospray Ionization Mass Spectrometer (ESI-MS) and Dynamic Light Scattering (DLS). The catalytic activity would be obtained by cyclic voltammogram. The bulk catalytic activity of hydrogen production process will be investigated in the further study.

1.4 Objectives

- 1.4.1 To post-modify poly(pentafluorophenyl acrylate) (poly(PFPA)) with aminothiophenol
- 1.4.2 To synthesize single-chain nanoparticles from the modified poly(PFPA) with suitable nickel precursor and its homogeneous analogues.
- 1.4.3 To synthesize and characterize homogeneous analogues.
- 1.4.4 To test the redox properties of the synthesized single chain nanoparticles and analogous homogeneous Ni(II) complexes.

1.5 Expected Result

The project will provide preliminary results of the synthesis and characterization of SCNPs and related homogeneous catalysts for hydrogen production. Moreover, the redox properties of SCNPs and analogous homogeneous compounds will also be anticipated.

Chapter 2

Results and Discussions

As mentioned before, this project focused on creating of SCNPs based on the nickel cluster (**Chapter 1**) which has long known to be enzyme mimic. According to the precedent research, 1,1'-Bis(diphenylphospheny)ferrocene (dppf) supporting thiolate catalyst is very active towards hydrogen production.⁷ Hence, this design is incorporated into generating SCNPs as depicted in **Figure 2.1**.

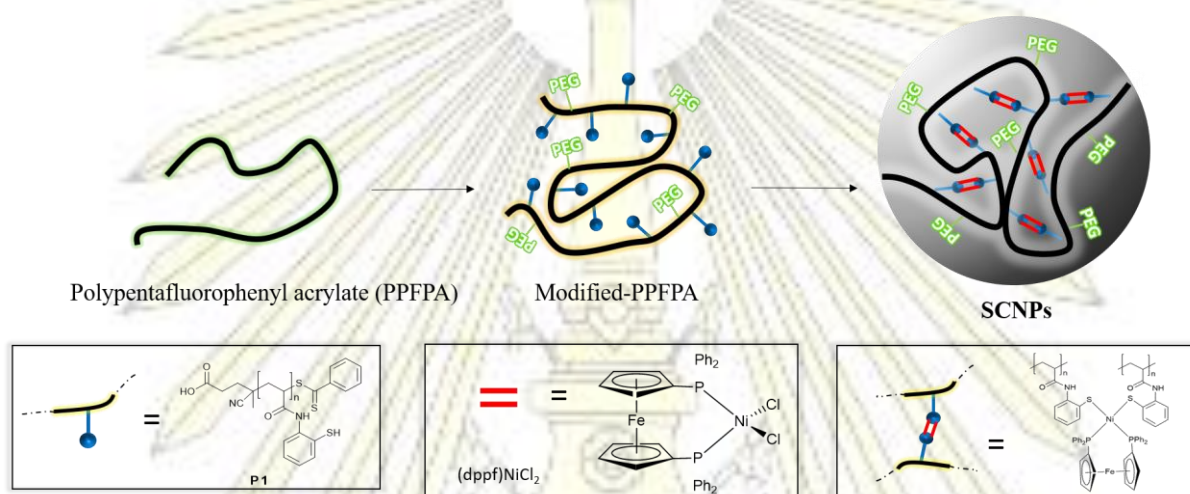
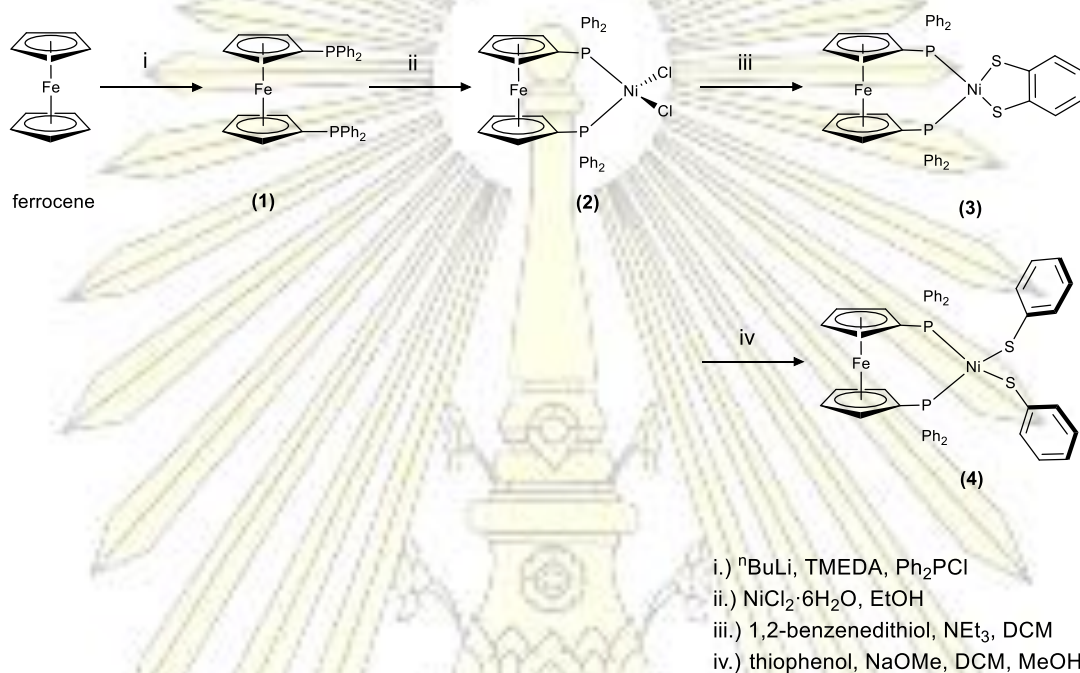


Figure 2.1 Illustration of Ni-SCNP via intramolecular crosslinking of modified poly(PFPA) by metal-ligand complexation.

Along with the synthesis of the designed SCNPs shown in **Figure 2.1**, homogeneous analogues were synthesized to represent a smallest active unit in the SCNPs and to allow the molecular structure and catalytic activity to be compared with the SCNPs. As described about SCNPs formation in session 1.3, the chain folding process in this case occurs through the complexation between Ni(II) precursor and thiolate ligand on polymer. If the vicinal thiolate ligands on polymer were to bind with the nickel metal, this could be comparable to bidentate ligand and if the distant thiolate ligands on polymer were to bind with the nickel metal, it can be viewed as the separated monodentate thiolate ligands. Subsequently, two homologous catalysts, (dppf)Ni(S₂C₆H₄) and (dppf)Ni(SC₆H₅)₂, were synthesized to serve this investigation. In this chapter, the first half will explain about the synthesis and structural characterization including catalytic activity of homogeneous complex using a cyclic voltammetry technique and the later half of this chapter will show the post-polymerization modification and the formation of SCNPs.

2.1 Synthesis of Ferrocene-derivative Compounds

Analogous complexes were synthesized by salt metathesis reaction between the corresponding nickel dichloride complex and appropriate thiol with the use of base, whereby this nickel complex precursor has been made from 1,1'-Bis(diphenylphospheny)ferrocene and $\text{NiCl}_2 \cdot 6\text{H}_2\text{O}$ as shown in general **Scheme 2.1**



Scheme 2.1 The synthetic routes for ferrocene-derivative compounds: dppf (**1**), $(\text{dppf})\text{NiCl}_2$ (**2**), $(\text{dppf})\text{Ni}(\text{S}_2\text{C}_6\text{H}_4)$ (**3**) and $(\text{dppf})\text{Ni}(\text{SC}_6\text{H}_5)_2$ (**4**).

2.1.1 The Synthesis of 1,1'-Bis(diphenylphospheny)ferrocene (dppf, 1)

Ferrocene derivative **1** was synthesized via a nucleophilic substitution reaction through a lithiated ferrocene. ${}^n\text{BuLi}$ and its stabilizer TMEDA were slowly added to a solution of ferrocene in anhydrous hexane at -78°C under a nitrogen atmosphere due to the exothermic reaction. Then, 2 equivalents of Ph_2PCl was added to form 1,1'-Bis(diphenylphospheny)ferrocene (dppf). The reaction was quenched with water to decompose all the lithiating agents in the solution and extracted with DCM. The crude product was purified using column chromatography by hexane/ CH_2Cl_2 49:1 gradient to 1.5:1 to remove lithiated ferrocene and 1-(diphenylphosphynyl)-1'-lithiumferrocene. The product yield was moderate as 42% yield due to the sequence methods of reaction and purification.

^1H NMR was used to characterize the purified product. According to the symmetrical structure of **1**, ^1H NMR detected the significant resonances as shown in **Figure 2.2**. A resonance at δ 7.22 ppm (**a**) appearing at the region of aromatic proton belongs to the 20 protons of 4 phenyl rings. The resonances **b** and **c** (δ 4.20 and 3.94 ppm) belong to each 4 protons at position α and β of Cp rings, respectively.

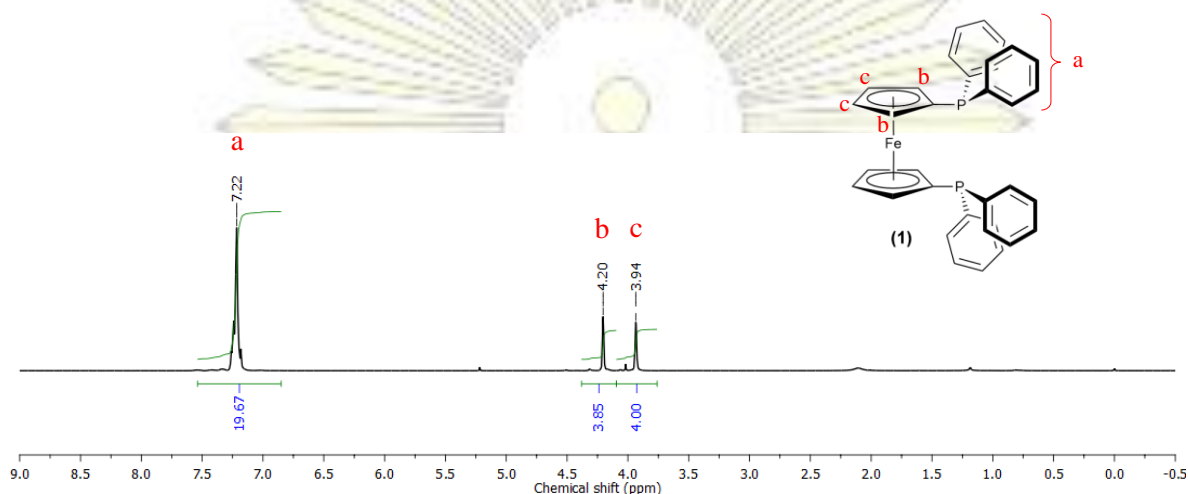


Figure 2.2 ^1H NMR (400.0 MHz, CDCl_3 , 298 K) of 1,1'-bis(diphenylphosphanyl)ferrocene (**dppf,1**).

UV-Visible spectra displayed only the absorbance at ultraviolet region (λ_{max} 232 nm ($\epsilon = 24\,500\ \text{M}^{-1}\ \text{cm}^{-1}$) and λ_{max} 251 nm ($\epsilon = 22\,383\ \text{M}^{-1}\ \text{cm}^{-1}$)) owing to absorption of electrons of the ferrocene unit. IR spectra showed low intensity peak except the overtone of aromatic, weak peak of C-H stretching at approximately $3000\ \text{cm}^{-1}$ and C=C stretching at 1582 and $1474\ \text{cm}^{-1}$. Mass spectrum using electrospray ionization source reported $554\ \text{m/z}$ of $[\text{dppf}]^+$, $555\ \text{m/z}$ of $[\text{dppf} + \text{H}]^+$ and $593\ \text{m/z}$ of $[\text{dppf} + \text{K}]^+$. The elemental analysis examined percentages of C and H found in the molecular structure as 73.60 and 4.91, respectively. The calculation data of C and H was 73.66 and 5.09, respectively. Both results showed the consistent number of elements which can confirm the bulk purity of this material.

2.1.2 The Synthesis of (dppf)NiCl₂ (2)

(dppf)NiCl₂ was synthesized via complexation reaction between **1** and nickel chloride hexahydrate (NiCl₂·6H₂O). All reagents were dissolved in anhydrous EtOH under nitrogen atmosphere at RT. Due to the volatility of solvent, the reaction was refluxing at 80°C for 2 h to ensure the completion. The color of slurry changed from orange to dark green which is unique in forming of complex compound. The crude product was filtered and washed with cold EtOH and diethyl ether to remove impurities as unreacted reagents and byproducts (**1**, NiCl₂·6H₂O and water). All volatiles were removed under *vacuo* to obtain the product as a dark green powder with 86% yield. The quantity of product was high because the coordination complex can form easily by $p\pi-d\pi$ interaction, which the phosphorus atom as a Lewis base donated pair of electrons to d-orbitals of nickel ion possessing Lewis acid properties.

Crystallographic data of this complex (**2**) was reported by Casellato.³⁰ The nickel complex possesses the tetrahedral structure around the metal center, hence the d⁸-compound presented a strong paramagnetism. NMR techniques reported the unexpected chemical shifts (*vide infra*). Therefore, ¹³C{¹H} and ³¹P{¹H} NMR data were omitted in this case. IR spectrum did not exhibit the signal of NiCl₂. The C-H stretching, overtone of aromatic and C=C stretching peaks (1482 and 1434 cm⁻¹) still appeared at the approximately same wavenumbers. UV-Vis spectra showed an extra absorbance at λ_{\max} 404 nm which is the visible wavelength of electromagnetic wave with the molar absorptivity, $\epsilon = 1593 \text{ M}^{-1} \text{ cm}^{-1}$. According to the high dilution to 100 μM of this compound before measurement, the solution's color is yellow-green. (**Figure 2.3**) So, the wavelength of absorption was magenta and the color appear to eyes was green to yellow.

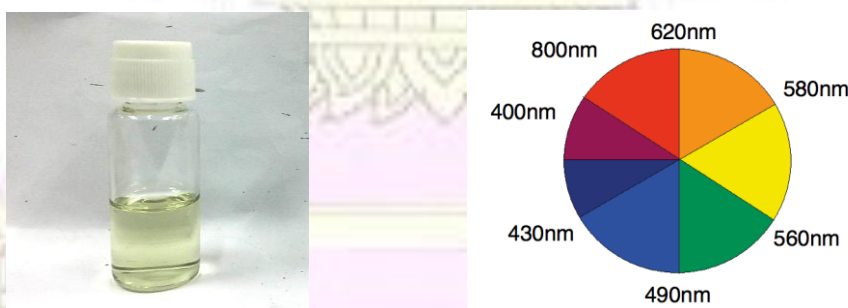


Figure 2.3 Sample solution of (dppf)NiCl₂ for UV-Vis measurement (left) The complementary color circle in different wavelength (right).

Moreover, elemental analysis showed the amount of C and H as 59.77 and 3.98%, respectively. From the calculation data, C and H was 59.71 and 4.13%, respectively. Both data predicted the same number of elements.

2.1.3 The Synthesis of (dppf)Ni(S₂C₆H₄) (3)

(dppf)Ni(S₂C₆H₄) was synthesized via a ligand substitution reaction of 1,2-benzenedithiol and **2**. After all reagents were dissolved in anhydrous DCM, triethylamine (NEt₃) was added as a strong base to deprotonate hydrogen atom at thiol group. The reaction completed within 2 h before removing all volatiles under *vacuo*. The crude product was washed with water to get rid of remaining chloride ion (Cl⁻). To detect the chloride ions, the washed solution was tested with silver nitrate (AgNO₃) until no precipitation observed. After redissolved and dried, the obtained product was a brown powder with 43% yield.

The experimental data of ¹H NMR showed the resonances of each proton position with the supporting of ¹³C{¹H} NMR, Heteronuclear Multiple Bond Correlation (HMBC) and Heteronuclear Single Quantum Correlation (HSQC). Due to the structure was symmetrical, **Figure 2.4** will show only one proton position, which represents all the proton at the same position. The resonances at δ 7.93, 7.53 and 7.42 ppm belong to the protons of PPh₂ at *ortho*-*meta*- and *para*- position, respectively. The new resonances which appeared at δ 7.13 and 6.78 ppm were possessed by the α- and β- position of 1,2-benzenedithiol, respectively. Cyclopentadienyl ring's α- and β- protons was showed at the δ 4.41 and 4.25 ppm, respectively. All resonances are obvious and sharp which signify the loss of paramagnetism related the square planar structure.

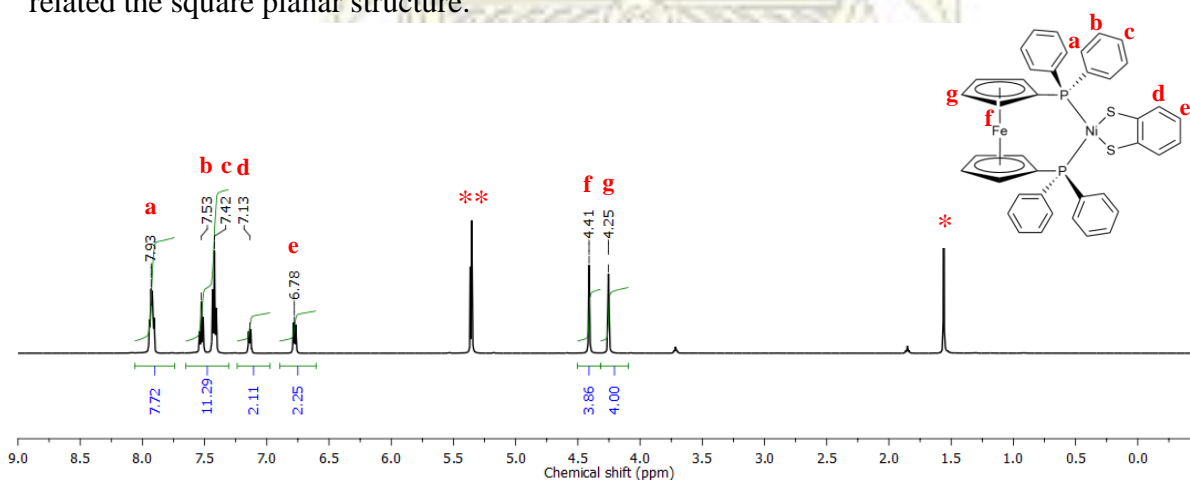


Figure 2.4 ¹H NMR (400.0 MHz, CDCl₃, 298 K) of (dppf)Ni(S₂C₆H₄) (**3**). An asterisk (*) and **) signifies the residue water and DCM, respectively.

UV-Vis spectrum reported the red shift of the absorbance from $\lambda_{\max} = 404$ nm of (dppf)NiCl₂ to $\lambda_{\max} = 410$ nm in the obtained product, which dilute to 100 μ M. The result related to the nature of compound, that was a brown color powder. According to the color circle (**Figure 2.3** (right)), the product absorbed the wavelength in the higher range and emitted another wavelength, which had higher intensity of yellow color. Mass spectrum showing the molecular weight of 777 m/z of [(dppf)Ni(S₂C₆H₄) + Na]⁺ supported the purposed molecular structure. Finally, elemental analysis and calculation data showed the percentage of C, H and S as 58.72 (58.75), 3.98 (4.09) and 7.72 (7.65), respectively. The results of both calculation related to the compound of (dppf)Ni(S₂C₆H₄) with DCM as a solvent of crystallization.

2.1.4 The Synthesis of (dppf)Ni(SC₆H₅)₂ (**4**)

Similar procedure and synthetic methodology was applied to **4**. In the synthesis of **4**, NEt₃ was employed as well as the milder sodium methoxide (NaOMe) in methanol was also used. Nevertheless, with similar reaction time to that of the synthesis of **3**, the crude product showed multiple species as illustrated by ³¹P{¹H} NMR spectra. (**Figure 2.5**)

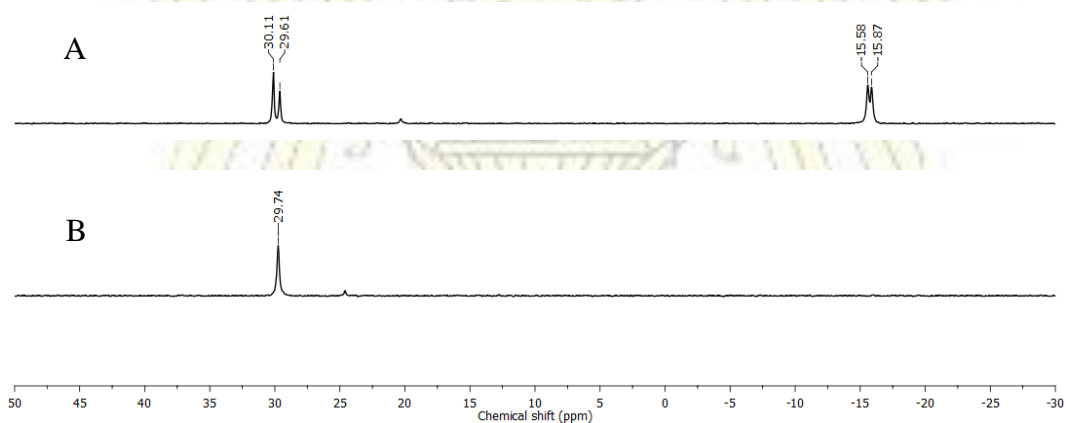
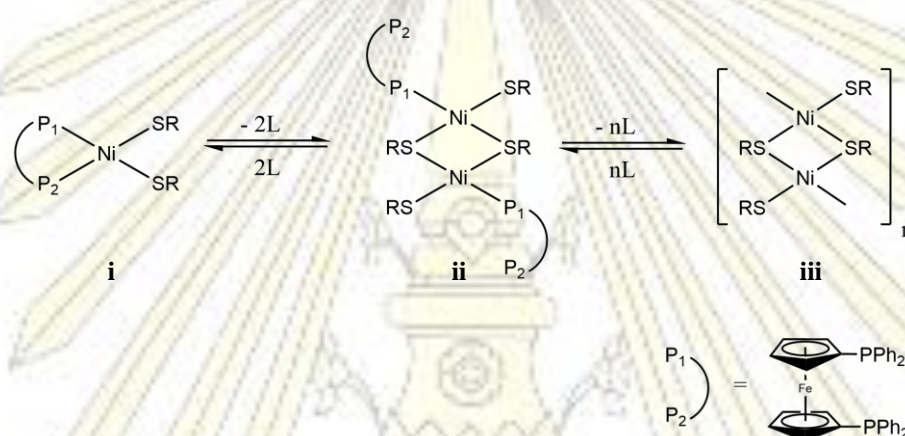


Figure 2.5 ³¹P{¹H} NMR (161.9 MHz, CDCl₃, 298 K) of **4** at 2 h (A) and 24 h (B).

It is known that phosphine supporting group 8 thiophenolate may not be stable. This compound could be in equilibrium as shown in **Scheme 2.2**. The 4-proposed species shown in **Scheme 2.2** corresponded to the 4 resonances of $^{31}\text{P}\{^1\text{H}\}$ NMR at δ 30.1 (P_1 in **ii**), 29.6 (P_1 and P_2 in **i**), 15.8 (P_2 in **ii**) and 15.5 (free ligand as a counter part of **iii**) ppm. An NMR tube-scale solution of crude product of **4** in CDCl_3 was left standing at RT for 3 days. Precipitate was observed at the bottom of the tube. The solution showed only one signal appearing at δ 29.7 ppm. The ^1H NMR of compound **4** in solution was fully characterized shown in **Figure 2.6**. The precipitate was suspected as oligomeric form of Ni-S bridge and oxidized form of free ligand which was found in single crystallography (The crystal of impurity was not presented in this report).



Scheme 2.2 Equilibrium between the possible structure of monomeric nickel thiolate compound and oligomeric Ni-S bridged compound.³¹

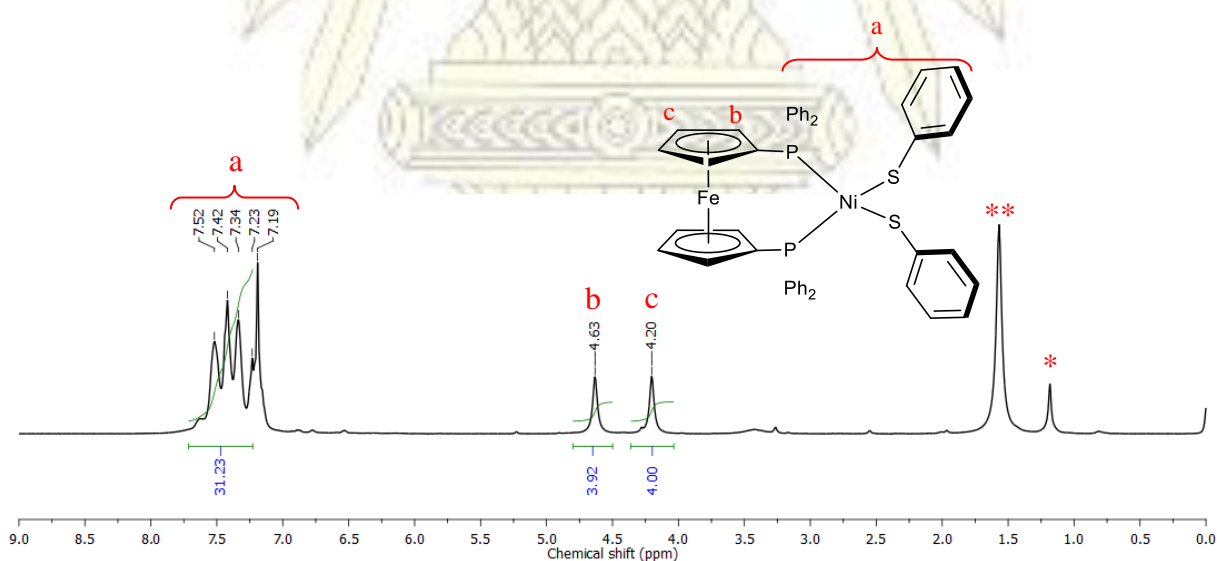


Figure 2.6 ^1H NMR (400.0 MHz, CDCl_3 , 298 K) of $(\text{dppf})\text{Ni}(\text{SC}_6\text{H}_5)_2$ (**4**). An asterisk (*) and **) signifies the residue grease and water, respectively.

2.2 The Study of Redox Behavior of Compound 3 and Its Reactivity Towards Hydrogen Evolution

Cyclic voltammograms of **3** was performed in DMF with an electrolyte, TBAPF₆, under nitrogen atmosphere at 100 mV/s. As shown in **Figure 2.7**, a reversible reduction at -1.580 V belongs to the reversible redox activity Ni^{II}/Ni^I without the decomposition of the compound. An oxidation peak at +0.3349 V belongs to the partial reversible Fe^{II}/Fe^{III} of dppf ligand. At this point, the decomposition of dppf compound was observed.

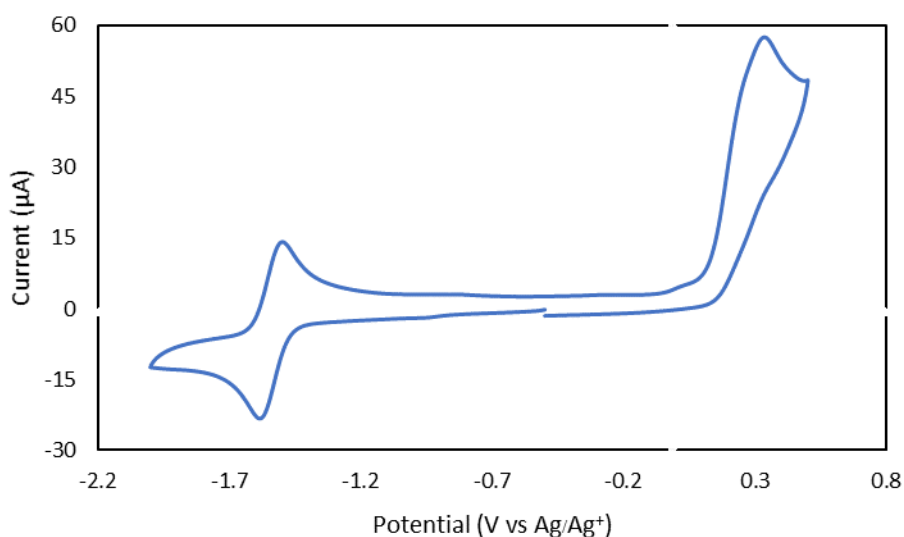


Figure 2.7 Cyclic voltammogram of **3** in DMF at a potential scan rate of 100 mV/s.

Then, the reactivity of **3** towards hydrogen production was tested by an addition of varying concentration of glacial acetic acid to the previous solution. (**Figure 2.8**) An increase of acid results in the enhancement in one direction of cathodic current at the potential of Ni^{II} reduction. This signifies that the production of hydrogen gas using compound **3** is feasible in DMF, although the signal enhancement in DMF may not be as high as that reported in THF.⁷

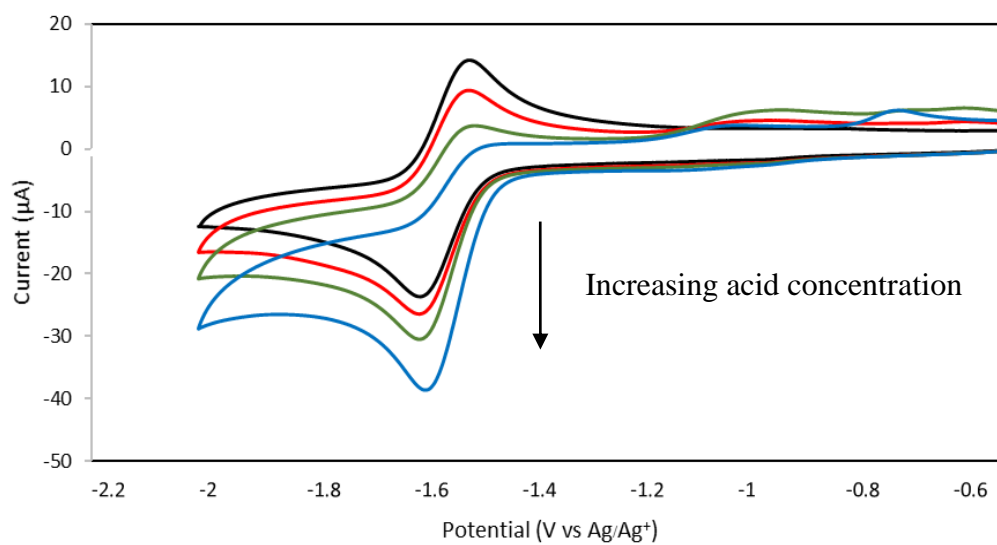


Figure 2.8 Cyclic voltammograms of **1** in the presence of varying concentration of acetic acid (CH_3COOH). The concentrations are 0, 32, 128 and 512 mM.

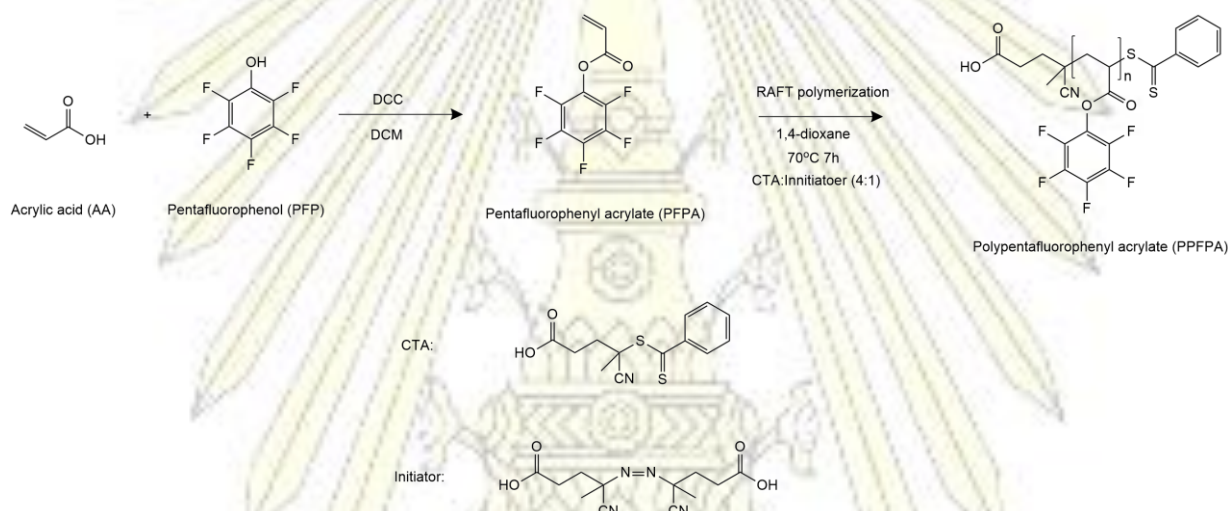


2.3 The Synthesis of Single Chain Nanoparticles (SCNPs)

The SCNPs studied in this project are based on the post functionalized polypentafluorophenyl acrylate (poly(PFPA)). The synthesis of poly(PFPA) by reversible addition-fragmentation chain-transfer or RAFT polymerization is convenient. This polymer has a high reactivity with amine group due to the higher nucleophilicity of the amine compared to the alcohol analogue. Moreover, pentafluorophenolate acts as a good leaving group.³²

2.3.1 The Synthesis of Poly(pentafluorophenyl Acrylate) (poly(PFPA))

The synthesis of poly(PFPA) was following the scheme below.



Scheme 2.3 The synthesis of PFPA (monomer) and poly(PFPA) via a RAFT polymerization.

By following the Jochum's method,³³ pentafluorophenyl acrylate (PFPA) was synthesized via a coupling reaction between acrylic acid (AA) and pentafluorophenol (PFP), whereby dicyclohexylcarbodiimide (DCC) as a coupling agent. The crude product was filtrated and passed through a column chromatography to remove a byproduct (dicyclohexylurea) and any unreacted reagents. The colorless liquid was obtained. The monomer was re-dissolved to perform a RAFT polymerization using 4-cyano-4-phenyl carbothioylthiopentanoic acid (CPADB) as a chain transfer agent (CTA) and 4,4'-azobis(4-cyanovaleric acid) (ACVA) as an initiator with ratio of 4:1. (**Scheme 2.3**) The reaction was performed in specific time (7 h) to gain the precise molecular weight of polymer product. The

pink powder product was purified by precipitation in different polarity solvent such as methanol to yield 70% product.

The purified product was characterized by ^1H NMR spectroscopy; the end group proton resonances (a) appear at the chemical shift of δ 7.90-7.40 ppm. The polymeric backbone protons resonances (b and c) are in range of δ 3.50-1.75 ppm as indicated in **Figure 2.9**. To specify the exact position, proton b appears in the more downfield position compared to c due to the presence of nearby carbonyl of an ester group exerting the inductive electron-withdrawing effect. In addition, the integration of b is halved to that of c, the characterization is consistent with the polymer backbone protons and also confirmed with the 2-dimensional ^1H - $^{13}\text{C}\{^1\text{H}\}$ experiment.

To calculate the degree of polymerization (DP), the integral resonances labelled 'a', corresponding to the aromatic proton of the end group, is set to 5, and the DP can be obtained directly from the integration of resonance b. In this case, the DP of poly(PFPA) product is 90 and the molecular weight is equal to $21700\text{ g}\cdot\text{mol}^{-1}$. It should be noted that the NMR calculation was the only available method to gain the molecular weight of the polymer during the time the study was conducted.

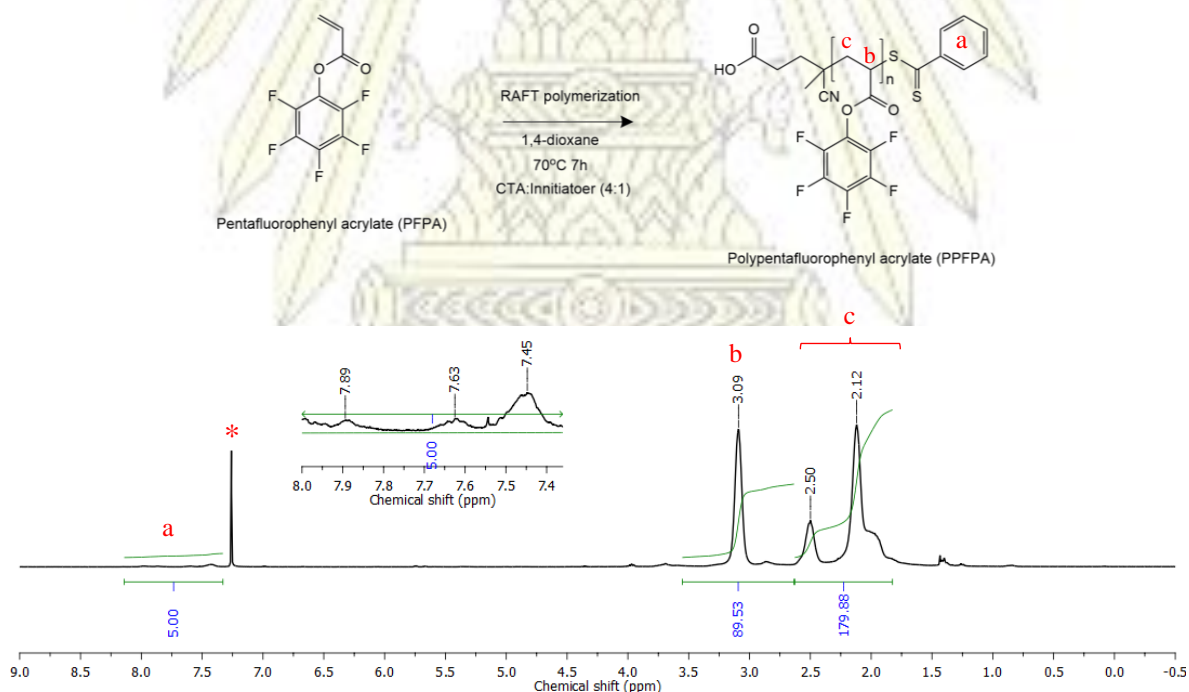
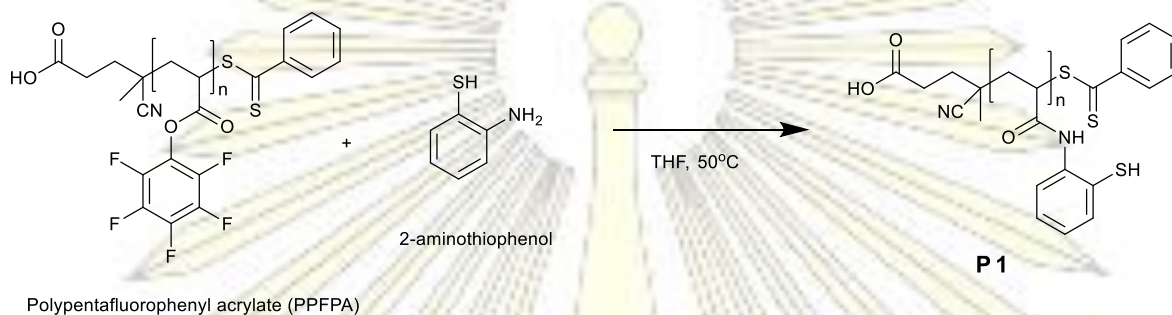


Figure 2.9 ^1H NMR spectrum (400.0 MHz, CDCl_3 , 298 K) of poly(PFPA). An asterisk signifies the residue protio- CHCl_3 from the NMR solvent.

2.3.2 The Synthesis of Modified Poly(PFPA)

To imitate the reported structures of [Ni-Fe] enzymes and catalysts mentioned in chapter 1, the incorporation of aminothiophenol to the poly(PFPA) was sought after. The synthesis of modified poly(PFPA) followed the scheme below. The feasibility of this reaction is an aminolysis of anime group to a carbonyl of active ester.



Scheme 2.4 The modification of poly(PFPA) with 2-aminothiophenol (**P1**).

The modified polymer was synthesized following **Scheme 2.4** by a substitution reaction of pentafluorophenol in poly(PFPA) with 2-aminothiophenol with the ratio of poly(pentafluorophenyl acrylate) to 2-aminothiophenol equals to 1:1.5. The reaction was carried out in THF at 50°C. The solution sample was taken at the specific time at 2 h, 17 h and 22 h to determine the degree of functionalization using $^{19}\text{F}\{^1\text{H}\}$ NMR spectroscopy (**Figure 2.10**). $^{19}\text{F}\{^1\text{H}\}$ NMR spectra also show broad resonances of pentafluorophenyl ring on the poly(PFPA) at δ 153.7, 158.4 and 163.1 ppm and sharp resonances at δ 164.4, 165.4 and 170.4 ppm belonged to free pentafluorophenol molecule. The integration of **a** and **A** was used to calculate the degree of functionalization as stated in equation (1). From the calculation, the degree of functionalization reaches 60% within 22 h.

$$\text{Degree of functionalization} = \frac{\int A}{\int A + \int a} \times 100 \quad (1)$$

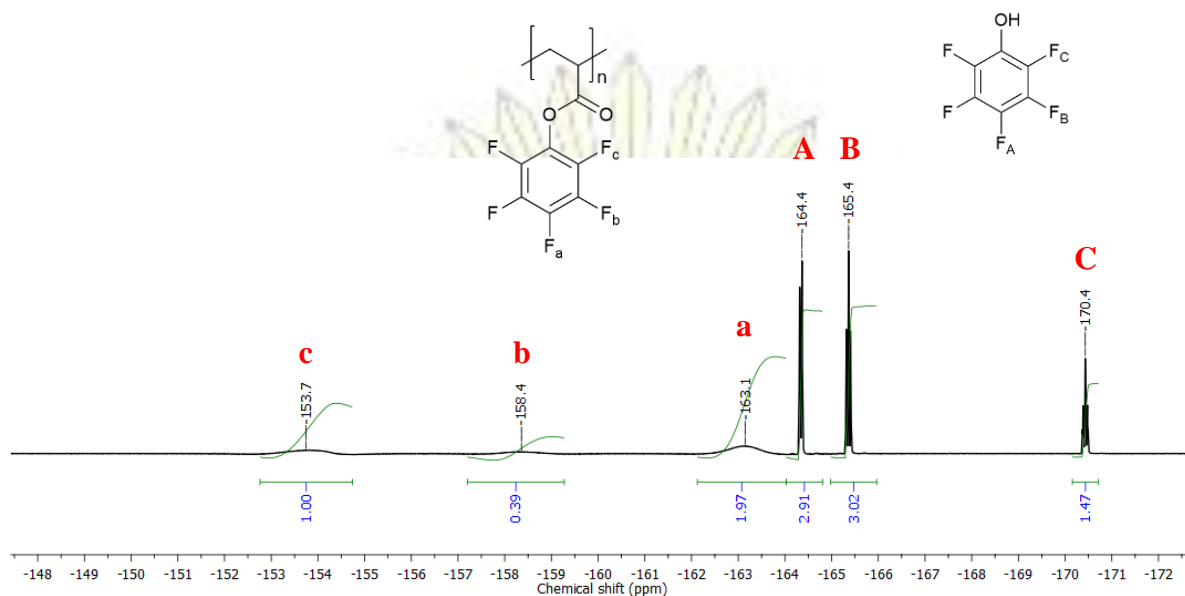


Figure 2.10 $^{19}\text{F}\{^1\text{H}\}$ NMR (376.5 MHz, CDCl_3 , 298 K) of crude modified poly(PFPA) at 22 h.

The observation of product forming can be clearly detected by naked-eye due to the color changed from pale pink to pale yellow solution. The crude product was purified by precipitation in hexane. After that, all volatiles were removed under *vacuo* leaving the polymer product.

Although the change in $^{19}\text{F}\{^1\text{H}\}$ NMR measurement was observed and meaningful, the ^1H NMR analysis gave no useful information, only some broadening on backbone resonances was observed.

The precedent literatures³⁴⁻³⁵ suggested the possibility of the products formation picturized in **Figure 2.11** due to the feasibility of nucleophilic substitution of $-\text{SH}$ and NH_2 . IR spectrometer was used to analyze the functional groups in the polymer product. The IR measurements were recorded for both poly(PFPA) and modified one. (**Figure 2.12**) The broad peak at wavenumber 3393 cm^{-1} belongs to S-H stretching of thiol group in modified poly(PFPA), (red, **Figure 2.12**). which does not observe in poly(PFPA) spectra (blue, **Figure 2.12**). The carbonyl ($\text{C}=\text{O}$ stretching) of ester group appear as a medium peak at the wavenumber of 1780 cm^{-1} in both spectra, however the intensity was diminished in the spectrum of poly(PFPA) owing to its 60% functionalization. A new peak at the wavenumber of 1692 cm^{-1} signifies the carbonyl of a new amide bond in the modified poly(PFPA) spectra. The absence of the peak corresponding to the $\text{C}=\text{N}$ stretching at the wavenumber of

1600 cm^{-1} ³⁶ and the C=O stretching frequency of thioester at wavenumber of 1708 cm^{-1} ,³⁷ confirms that the obtained poly(PFPA) is in form of structure **i** in **Figure 2.12**.

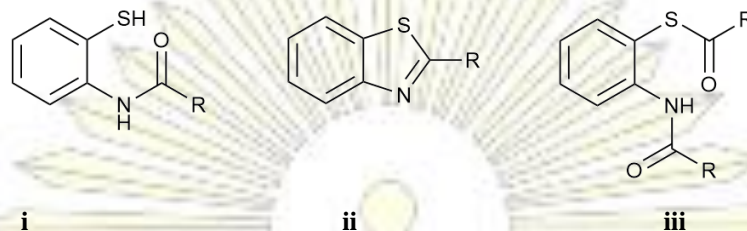


Figure 2.11 Possible products formed in the modification of poly(PFPA) with 2-aminothiophenol (R is polymeryl group).

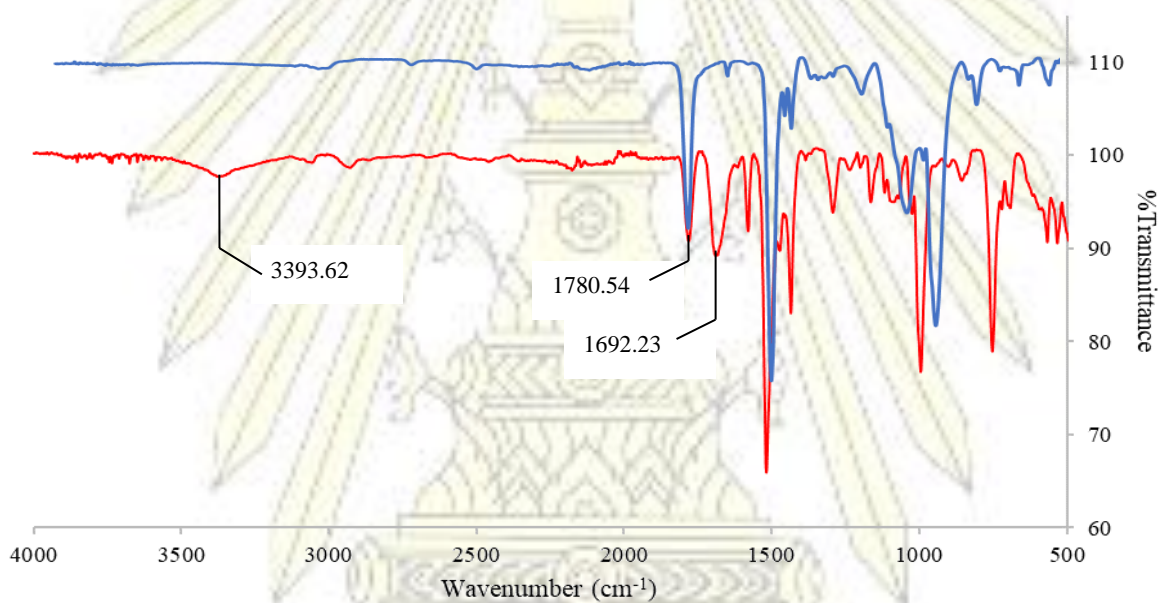


Figure 2.12 Stacked IR spectra of poly(PFPA) (blue) and modified poly(PFPA) with 2-aminothiophenol (red).

Aside from 2-aminothiophenol, the post-polymerization modification of poly(PFPA) was carried out with 3-aminothiophenol. The same synthetic procedure and condition was applied. As previously mentioned, $^{19}\text{F}\{^1\text{H}\}$ NMR spectroscopy was used to examine the degree of functionalization. Nevertheless, the conversion from poly(PFPA) to modified poly(PFPA) with 3-aminothiophenol was negligible within the same period of reaction time. It could be concluded that the modification with 3-aminothiophenol was unsuccessful.

As described, the reaction of poly(PFPA) with 2-aminothiophenol outperformed the analogous reaction with 3-aminothiophenol. It is not trivial to quantify and compare the nucleophilicity of the amino group in 2- and 3-aminothiophenol as both are influenced by the electron donating mesomeric effect and the electron withdrawing inductive effect of the nearby thiol substituent. The enhanced reactivity observed could be explained in a term of stability of tetrahedral intermediates formed during the reaction (**Figure 2.13**). The positive charged ammonium can be stabilized better with thiol group in an *ortho* position. To sum up, the modification of poly(PFPA) with aminothiophenol was successful, however only with 2- or 4-aminothiophenol. The rate of reaction is significantly slower compared to the similar poly(PFPA) modification with primary amine.³²

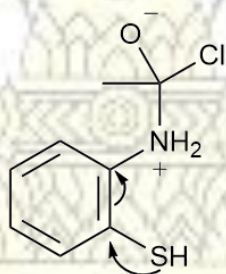


Figure 2.13 Nucleophilic substitution intermediate of 2-aminothiophenol.

2.3.3 The Synthesis of Single Chain Nanoparticles of Modified Poly(PFPA)

Single chain nanoparticles of modified poly(PFPA) was synthesized by metal-ligand complexation between the functional polymer (**P1**) and **2**. As illustrated in **Figure 2.1**, the stoichiometric ratio of thiol functionalized poly(PFPA) to **2** equals to 2. The reaction conducted within very dilute condition (1 mg/mL). Both reagents were dissolved in THF before adding NEt_3 dropwise in an excess equivalent to allow the complex formation. The stirred solution changed its color from pale green to brown immediately. The reaction was left stirred at RT for 10 mins before the UV-Vis spectrometer was used to detect the formation of nanoparticles. As shown in **Figure 2.14**, compound **2** gave a peak at 404 nm where the intensity diminished when NEt_3 was added. This implied the change of precursor **2** into the new species of which SCNPs is expected. The decrease of signal intensity when higher equivalent of base was added upto a uniequivalent to $[\text{Ni}^{2+}]$ assumed to be due to the more compact size of SCNPs produced. The more compact particles behave less absorption.

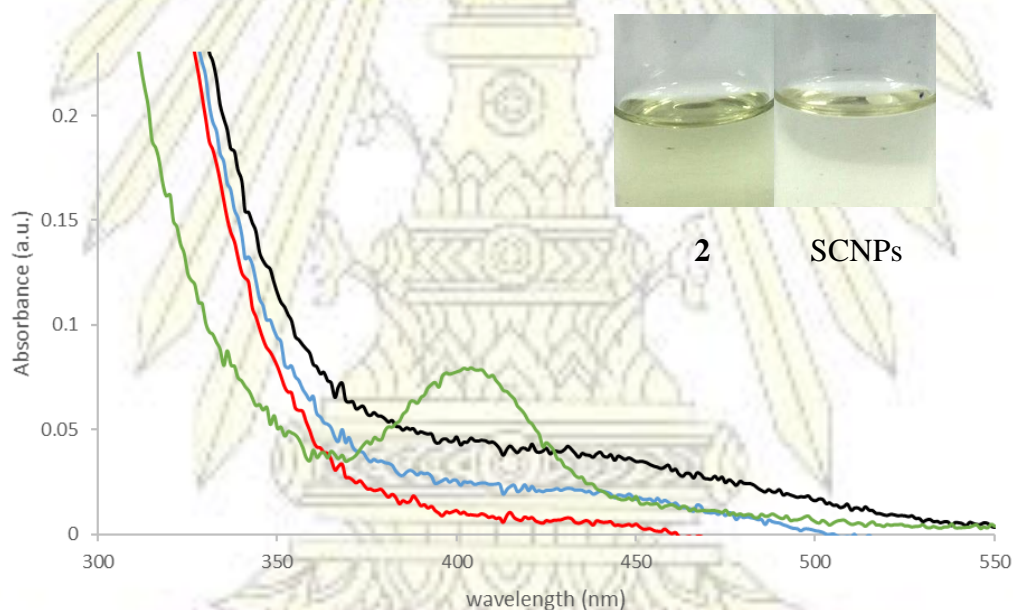


Figure 2.14 UV-Vis spectra at RT of **2** (green) and SCNPs with adding amount of NEt_3 2.4 μL (0.3eq. to $[\text{Ni}^{2+}]$) (black), 4.8 μL (0.6 eq. to $[\text{Ni}^{2+}]$) (blue) and 7.2 μL (1.0 eq. to $[\text{Ni}^{2+}]$) (red).

The solution of SCNPs was concentrated under *vacuo* and put in NMR tube. $^{31}\text{P}\{^1\text{H}\}$ NMR was used to investigate the formation of SCNPs and we found that NMR results showed the crosslinking between thiolate ligands and nickel ions as a comparison with the resonances of compound **4**. To sum up, the linkage between Ni-S on the polymer was formed, however defined thiolate and bridging thiolate were both assumed.

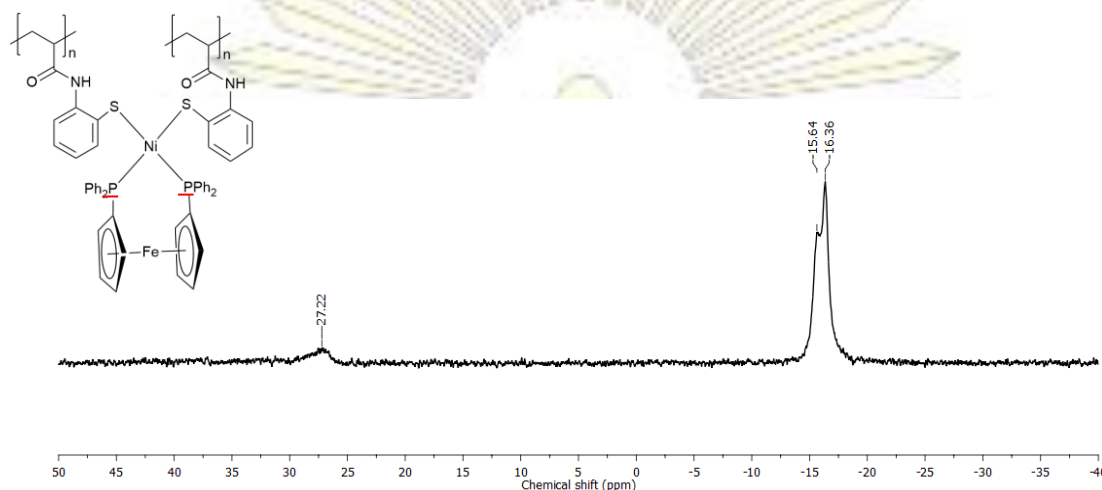


Figure 2.15 $^{31}\text{P}\{^1\text{H}\}$ NMR (161.9 MHz, 10% CDCl_3 in THF-H_8 , 298K) of crude SCNPs.

The micrographs recorded by TEM showed the size of SCNPs in a very dilute condition to be approximately 30 to 50 nm of smaller nanoparticles as shown in red circles in **Figure 2.16** and 700-2000 nm of the aggregated SCNPs after left standing for a week. The denser area of the SCNPs aggregation belongs to the metal complex whilst the less dense area belongs to the polymeric chain. In the same way, DLS data supported the nano-sized of the obtained particles and their aggregation as 35 nm (**Figure 2.17**) and 708 nm (**Figure 2.18**), respectively. According to the DLS and TEM results, they showed the physical properties which can confirm the formation of SCNPs.

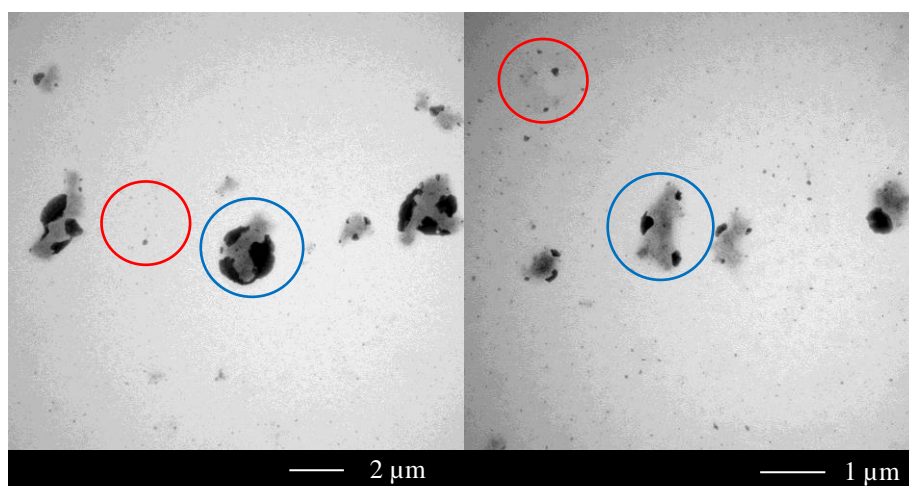


Figure 2.16 TEM micrographs of SCNPs (red circle) and their aggregation (blue circle).

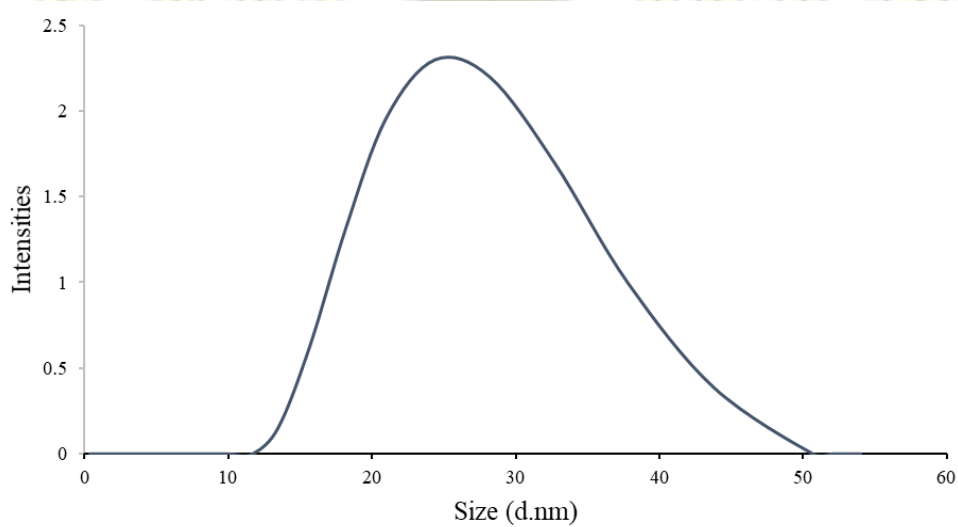


Figure 2.17 DLS spectrum of SCNPs.

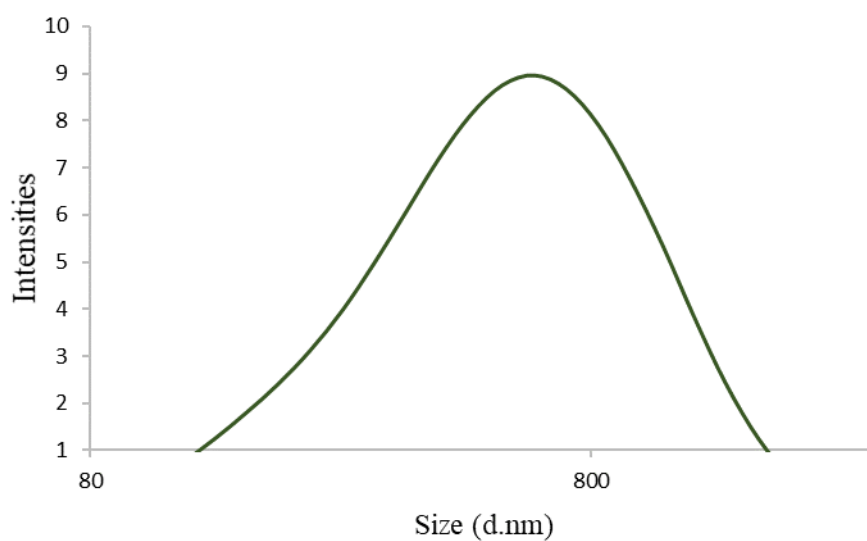


Figure 2.18 DLS spectrum of aggregated SCNPs.

These preliminary results confirm the formation of SCNPs, however the further synthetic strategies need the bulky either thiophenolate group or nickel complex to prevent the bridging formation and other modified group to increase the water solubility property to the SCNPs. The catalytic activity of hydrogen production will be studied in the further experiment.

Chapter 3

Experimental

3.1 Materials and Instruments

3.1.1 Materials

All manipulations were carried out using standard Schlenk line technique under an inert atmosphere of nitrogen. All glasswares were dried at 110 °C for 24 h and cooled under vacuum prior to use. Solvents were purchased as anhydrous or dried by passing through a column of appropriate drying agent, and stored under nitrogen atmosphere, over 4 Å molecular sieves.

All solvents and reagents for the synthesis of ferrocene derivatives were obtained from commercial sources (Alfar Aesar, VWR International and Sigma-Aldrich) and used as received unless stated otherwise. Solid reagents were stored under an inert atmosphere of nitrogen in a glovebox, whilst liquid reagents were stored in rota-flow ampoules under an inert atmosphere of nitrogen. All solvents used in working-up steps for the synthesis of ferrocene derivatives are analytical grade. 1,1'-Bis(diphenylphosphino)ferrocene (dppf, **1**),³⁸ (dppf)NiCl₂ (**2**),³⁹ (dppf)Ni(S₂C₆H₄) (**3**),⁴⁰⁻⁴¹ and (dppf)Ni(S₂C₆H₄) (**4**)⁴²⁻⁴³ were prepared according to or adapted from literature procedures.

All solvents for the synthesis of pentafluorophenol (PFPA) and poly(PFPA) were analytical grade and used as received. 1,4 Dioxane (anhydrous, 99.9%), pentafluorophenol (PFP) and 1-amino-2-propanol were commercially available from Merck, Germany. Dichloromethane (DCM) was dried over CaH₂ and reflux under N₂ atmosphere before use. 4,4'-azobis (4-cyanovaleric acid) (ACVA), dicyclohexylcarbodiimide (DCC) and anhydrous N,N'-dimethyl formamide (DMF, 98.8%) were obtained from Sigma-Aldrich, USA. Acrylic acid (AA) was purchased from Sigma-Aldrich, USA and distilled under vacuum before use. 4-cyanopentanoic acid dithiobenzoate (CPADB) was obtained from Santa Cruz Biotechnology, USA.

3.1.2 Instruments

Nuclear Magnetic Resonance (NMR). ^1H , $^{13}\text{C}\{^1\text{H}\}$, $^{19}\text{F}\{^1\text{H}\}$, $^{31}\text{P}\{^1\text{H}\}$ and 2D NMR spectra were recorded using the Bruker AV400 or AVD500 MHz spectrometer at ambient temperature. ^1H , $^{13}\text{C}\{^1\text{H}\}$, $^{19}\text{F}\{^1\text{H}\}$, $^{31}\text{P}\{^1\text{H}\}$ NMR spectra were referenced internally to residue protio-solvent (^1H). $^{13}\text{C}\{^1\text{H}\}$, $^{19}\text{F}\{^1\text{H}\}$, $^{31}\text{P}\{^1\text{H}\}$ resonances are reported relative to tetramethylsilane (TMS), trichlorofluoromethane (CFCl_3) and 85% phosphoric acid (H_3PO_4), respectively. Mestrenova software (version 6.0.2) was used to process and analyze the spectra.

Dynamic Light Scattering (DLS). The DLS measurements were conducted using a Zetasizer Nano series instrument (the Malvern Instrument Zen 1600). The scattering angle was set at 173° . All the aqueous aggregate solutions were dissolved in THF, filtered through a Millipore $0.45\ \mu\text{m}$ nylon membrane and put into quartz cuvettes for analysis.

Fourier Transform Infrared Spectrometer (FT-IR). All IR spectra were recorded by Fourier transform infrared spectrometer using the Perkin Elmer, Spectrum One instrument. The functional groups of all solid sample were determined with attenuated total reflectance (ATR) accessory at wavenumber range $4000\text{--}400\ \text{cm}^{-1}$.

UV-Visible spectroscopy (UV-VIS). All UV-Vis spectra were measured by the Varian Cary 50 Probe UV-Visible spectrometer using a UV Quartz Spectrometer Cuvette cell, path length 1 cm, volume 3.5 mL. All single site catalysts were dissolved in DCM with the concentration of $100\ \mu\text{M}$ and all polymer products were dissolved in THF with the concentration of $0.125\ \text{mg/mL}$. The 2.5 mL solution was injected to the cell by METTLER TOLEDO micropipette.

X-ray Crystallography. Crystals of the complex $(\text{dppf})\text{Ni}(\text{S}_2\text{C}_6\text{H}_4)$ were selected under an optical microscope and glued on glass fiber for single crystal X-ray diffraction experiments. X-ray diffraction data were collected using Bruker D8 QUEST CMOS using the Mo- $\text{K}\alpha$ radiation ($\lambda = 0.7107\ \text{\AA}$) and operating at $T = 296(2)\ \text{K}$. Data were measured using ω and ϕ scans of $0.5\ (\text{d}, \text{scan width})^\circ$ per frame for $30\ (\text{d}, \text{scan_rate})\ \text{s}$ using Mo- $\text{K}\alpha$ radiation (50 kV, 30 mA). The total number of runs and images was based on the strategy calculation from the program APEX3. Unit cell index was refined using SAINT (Bruker, V8.34A, 2013). Data reduction scaling and absorption corrections were performed using the SAINT (Bruker, V8.34A, 2013) and the SADABS-2014/4 (Bruker, 2014/4) was used for absorption correction.

Cyclic Voltammetry (CV). Cyclic voltammetric measurements were performed with the Autolab PGSTAT101 potentiostat/galvanostat (EcoChemie, The Netherlands) using a conventional three-electrode configuration. A glassy carbon electrode with a disk diameter of 3.0 mm was used as a working electrode. Before use, the electrode was polished with an aqueous suspension of alumina powder and rinsed thoroughly with Milli-Q water. A platinum wire was applied as an auxiliary electrode. All potentials are quoted with respect to non-aqueous silver/silver ion (Ag/Ag^+) reference electrode; this electrode was externally calibrated with a ferrocene/ferrocenium ion (Fc/Fc^+) redox couple and has a potential of 0.542 V versus a standard hydrogen electrode (SHE). Cyclic voltammograms of the Nickel complexes (2.00 mM) were recorded in a deoxygenated solvent (dimethylformamide, DMF) containing 0.10 M tetrabutylammonium hexafluorophosphate (TBAPF_6) at scan rates of 50-800 $\text{mV}\cdot\text{s}^{-1}$. The enhancement of current was verified by adding 1.0, 2.0, 4.0 8.0, 16.0 32.0, 64.0 and 128.0 mM of glacial acetic acid. A de-aeration procedure was carried out by purging with ultra-high purity (UHP) nitrogen.

Elemental Analysis. Percentage of C, H and S of compounds was measured using the CHNS/O THERMO, Elemental Analyzer. All samples were prepared as solid for analysis.

Electrospray Ionization Mass Spectrometer (ESI-MS). Mass spectrum list was reported by the micrOTOF-Q II 10355 mass spectrometer with an electrospray ionization (ESI) source type. The condition of nebulizer pressure, dry heater temperature and dry gas flow rate was set at 0.4 Bar, 200°C and 4.0 l/min. Mass range was scanned from 50 to 1500 m/z.

Transmission Electron Microscope (TEM). Micrographs of single chain nanoparticle were recorded by the Transmission Electron Microscope (TEM 1400) with the use of sodium (potassium) phosphotungstate (PTA) stain.

3.2 Experimental Procedures

3.2.1 Synthesis of ferrocene-derivative compounds

3.2.1.1 Synthesis of 1,1'-Bis(diphenylphosphenyl)ferrocene (dppf, 1)

N,N,N',N'-tetramethylethylenediamine (TMEDA, 1.95 mL, 12.0 mmols) and n-BuLi (7.39 mL, 11.84 mmols, 1.6 M in hexane) were added dropwise to a stirred solution of ferrocene (1.0 g, 5.38 mmols) in anhydrous hexane (20 mL) under a nitrogen atmosphere at RT. The solution was stirred at RT overnight. The orange slurry was allowed to settle, and the hexane layer was removed through a filter canula. The remaining orange powder was washed with anhydrous hexane (5 mL) and dissolved in anhydrous THF (10 mL). PPh₂Cl (2.37 mL, 14.79 mmols) was added to the orange solution at -78°C. The reaction was slowly warmed to RT. The reaction was left stirred for 5 h before quenched with water. The layer was separated and the aqueous was extracted thoroughly with DCM. The combined organic fractions were dried over Na₂SO₄ and evaporated under *vacuo* to give a crude product. The obtained product was purified using a flash chromatography to remove unreacted species by hexane/CH₂Cl₂ 49:1 gradient to 1.5:1. Yield 1.26 g (42% yield) as orange crystals. ¹H NMR (400.0 MHz, CDCl₃): δ 7.22 ppm (20 H, m, aromatic on phenyl), 4.20 ppm (4 H, s, α-Cp-H), and 3.94 ppm (4 H, s, β-Cp-H); ¹³C{¹H} NMR (100.6 MHz, CDCl₃): δ 139.0 ppm (PPh₂ C_{ipso}), δ 133.7 ppm (PPh₂ o-Ph), δ 128.9 ppm (PPh₂ m,p-Ph), δ 76.6 ppm (β-Cp), δ 74.0 ppm (α-Cp), δ 72.7 (Cp C_{ipso}); ³¹P{¹H} NMR (161.9 MHz, CDCl₃): -17.3 ppm; UV-Vis: λ_{max} 232 nm (ε = 24 500 M⁻¹ cm⁻¹) and λ_{max} 251 nm (ε = 22 383 M⁻¹ cm⁻¹); IR (ATR, cm⁻¹): 1582 (w), 1474 (m), 1428 (m), 1305 (w), 1193 (w), 1102 (m), 1091 (w), 1066 (w), 1024 (m), 827 (m), 740 (s), 695 (s), 632 (m); ESI-MS: 554 m/z ([dppf]⁺), 555 m/z ([dppf + H]⁺), 593 m/z ([dppf + K]⁺); Anal. Calcd. for C₃₄H₂₈FeP₂ (found): C, 73.60 (73.66); H, 4.91 (5.09).

3.2.1.2 Synthesis of (dppf)NiCl₂ (2)

1,1'-Bis(diphenylphosphenyl)ferrocene (0.70 g, 1.3 mmols) and nickel chloride hexahydrate (NiCl₂·6H₂O) (0.30 g, 2.3 mmols) were dissolved in anhydrous EtOH (20 mL) under a nitrogen atmosphere at RT. After stirring and refluxing at 80°C for 2 h, the slurry turned into dark green color. The crude was filtered and washed with cold EtOH and diethyl ether respectively. The obtained product was dried under *vacuo*. Yield 0.740 g (86% yield) as

a dark green powder. ^1H NMR (400.0 MHz, CD_2Cl_2): δ 20.65 ppm (s), 10.06 ppm (s), 4.22 ppm (s), and 3.96 ppm (s); Owing to the strong paramagnetic nature, $^{13}\text{C}\{^1\text{H}\}$ and $^{31}\text{P}\{^1\text{H}\}$ NMR characterization was omitted. UV-Vis: λ_{max} 404 nm ($\epsilon = 1593 \text{ M}^{-1} \text{ cm}^{-1}$); IR (ATR, cm^{-1}): 1586 (w), 1482 (m), 1434 (m), 1162 (m), 1097 (m), 1030 (m), 998 (w), 838 (m), 830 (m), 751 (m), 741 (s), 691 (s), 622 (m); Anal. Calcd. for $\text{C}_{34}\text{H}_{28}\text{FeNiP}_2\text{Cl}_2$ (found): C, 59.77 (59.71); H, 3.98 (4.13)

3.2.1.3 Synthesis of (dppf)Ni($\text{S}_2\text{C}_6\text{H}_4$) (3)

To a solution of (dppf)NiCl₂ (0.300 g, 0.44 mmols) in anhydrous DCM (20 mL) was added 1,2-benzenedithiol (67 μL , 0.58 mmols). Then, triethylamine (NEt_3) (0.7 mL) was added dropwise, all at RT. An immediate change in color from dark green to brown was observed. The reaction was left stirring for 2 h. After which time, all volatiles were removed under *vacuo*. The crude product was washed with a copious amount of water repeatedly. A chloride test was performed with silver nitrate (AgNO_3) solution until no precipitation of AgCl observed. The product was redissolved in DCM and dried over Na_2SO_4 . The solvent was removed under *vacuo* giving a crude product as a brown powder. The crude product was recrystallized in layered DCM/hexane solution. Yield 0.146 g (43% yield) as a brown powder. Diffraction-quality crystals were grown from a layered DCM/hexane solution at RT. ^1H NMR (400.0 MHz, CDCl_3): δ 7.93 ppm (8 H, m, *o*-PPh₂), 7.53 ppm (8 H, t, *m*-PPh₂), 7.42 ppm (4 H, t, *p*-PPh₂), 7.13 ppm (2 H, dd, α - $\text{S}_2\text{C}_6\text{H}_4$), 6.78 ppm (2 H, dd, β - $\text{S}_2\text{C}_6\text{H}_4$), 4.41 ppm (4 H, s, α -Cp-H), and 4.25 ppm (4 H, s, β -Cp-H); $^{13}\text{C}\{^1\text{H}\}$ NMR (100.6 MHz, CD_2Cl_2): δ 135.7 ppm ($\text{S}_2\text{C}_6\text{H}_4$ C_{ipso}), δ 135.6 ppm (*m*-PPh₂), δ 133.7 ppm (PPh₂ C_{ipso}), δ 131.2 ppm (*o*-PPh₂), δ 128.4 ppm (*p*-PPh₂), δ 127.0 ppm (β - $\text{S}_2\text{C}_6\text{H}_4$), δ 121.7 ppm (α - $\text{S}_2\text{C}_6\text{H}_4$), δ 76.2 ppm (α -Cp), δ 75.8 ppm (Cp C_{ipso}), δ 73.9 (β -Cp); $^{31}\text{P}\{^1\text{H}\}$ NMR (161.9 MHz, CD_2Cl_2): δ 26.9 ppm; UV-vis: λ_{max} 229 nm ($\epsilon = 91\,690 \text{ M}^{-1} \text{ cm}^{-1}$), λ_{max} 269 nm ($\epsilon = 57\,990 \text{ M}^{-1} \text{ cm}^{-1}$), λ_{max} 312 nm ($\epsilon = 38\,430 \text{ M}^{-1} \text{ cm}^{-1}$) and λ_{max} 410 nm ($\epsilon = 1288 \text{ M}^{-1} \text{ cm}^{-1}$); IR (ATR, cm^{-1}): 1478 (w), 1433 (m), 1264 (w), 1091 (m), 1027 (w), 813 (m), 738 (s), 689 (s), 634 (m); ESI-MS: 777 m/z ($[(\text{dppf})\text{Ni}(\text{S}_2\text{C}_6\text{H}_4) + \text{Na}]^+$) Anal. Calcd. for $\text{C}_{40}\text{H}_{32}\text{FeNiP}_2\text{S}_2 \cdot \text{CH}_2\text{Cl}_2$ (found): C, 58.72 (58.75); H, 3.98 (4.09); S, 7.72 (7.65)

3.2.1.4. Attempt to Synthesis of (dppf)Ni(SC₆H₅)₂ (4)

Compound **2** (0.100 g, 0.15 mmols) was dissolved in dry MeOH under a nitrogen atmosphere at RT. Thiophenol (32.0 μ L, 0.30 mmols) was added in to the stirred slurry dropwise by a micro syringe. Then, solution of sodium methoxide (NaOMe) (16.8 mg, 0.31 mmols) in MeOH was added dropwise. The reaction was stirring for 2 h. After which time, the color of the solution changed from dark green to brown. Crude product was dried under vacuum. ¹H NMR (400.0 MHz, CDCl₃): δ 8.00-7.20 ppm (30H, m, P(Ph-H)₂ and SC₆H₅), 4.70 ppm (4 H, s, α -Cp-H), and 4.28 ppm (4 H, s, β -Cp-H); ¹³C{¹H} NMR (100.6 MHz, CD₂Cl₂): δ 132.0-127.0 ppm (PPh₂ and S₂C₆H₄), δ 75.0-73.0 ppm (Cp); ³¹P{¹H} NMR (161.9 MHz, CD₂Cl₂): δ 29.7 ppm.

3.2.2 Synthesis of Single Chain Nanoparticles (SCNPs)

3.2.2.1 Synthesis of pentafluorophenyl acrylate (PFPA)

Pentafluorophenyl acrylate was synthesized according to the preparation reported by Jochum *et al.*³³ Pentafluorophenol (50.0 g, 0.27 moles) was dissolved in anhydrous DCM (10 mL) in a round bottom flask. The solution was stirred and cooled down in an ice bath. Then, acrylic acid (AA) (18.65 mL, 0.27 moles) was added dropwise into the solution. Dicyclohexylcarbodiimide (DCC) (56.04 g, 0.27 moles) was dissolved in anhydrous DCM (10 mL) and added into the previous mixture. The solution was stirred for 2 h. A white precipitate of dicyclohexylurea was removed by *vacuo* filtration and washed with DCM. The filtrate was evaporated to obtain the crude product. Subsequently, the crude was purified by column chromatography with hexane. Colorless liquid was obtained. Yield 45.2 g (70% yield). ¹H NMR (400.0 MHz, CDCl₃): δ 6.73 ppm (1 H, d, *cis*-H), 6.38 ppm (1 H, m, *trans*-H), 6.19 ppm (1 H, d, *vic*-H). ¹⁹F NMR (376.5 MHz, CDCl₃): δ -162.77 ppm (d, 2F), δ -158.39 ppm (t, 1F), δ -153.02 ppm (d, 2F).

3.2.2.2 Synthesis of poly(pentafluorophenyl acrylate) (poly(PFPA))

Poly(pentafluorophenyl acrylate) (poly(PFPA)) was synthesized *via* a reversible addition-fragmentation chain transfer or RAFT polymerization.⁴⁴ PFPA (2 M) was dissolved in dioxane (2 mL) in a glass vial. Then, 1 mL of dioxane containing initiator, 4,4'-azobis (4-cyanovaleric acid) (ACVA, 33.5 mg, 0.12 mmol), and RAFT agent, 4-cyano-4-(thiobenzoylthiol) pentanoic acid (CPADB, 8.4 mg, 0.03 mmol) were added into the solution.

Subsequently, the vial was sealed and stirred under a nitrogen atmosphere for 30 min. Then, the vial was immersed in a preheated oil bath at 70°C for 7 h. The final solution was cooled down to the RT and precipitated in methanol and THF in methanol, respectively. Pink powder product was obtained. ^1H NMR (400.0 MHz, THF- d_8): δ 7.89 ppm (1 H, b, aromatic of end group), 7.63 ppm (2H, b, aromatic of end group), 7.45 ppm (2 H, b, aromatic of end group), 3.09 ppm (90 H, s, polymer backbone C_{ipso}), 2.50-2.12 ppm (180 H, m, polymer backbone $\alpha\text{-CH}_2$); degree of polymerization (DP): 90 (calcd. from ^1H NMR integration); $^{19}\text{F}\{^1\text{H}\}$ NMR (376.5 MHz, CDCl_3): δ -154.4 ppm (ring residue), δ -158.0 ppm (ring residue), δ -163.5 ppm (ring residue); IR (ATR): 1781 (m), 1514 (s), 1079 (m), 987 (s).

3.2.2.3 Synthesis of modified poly(PFPA) with 2-aminothiophenol

Poly(PFPA) (0.300 g, 0.012 mmols) was dissolved in anhydrous THF at RT under a nitrogen atmosphere. 2-aminothiophenol (200 μL , 1.88 mmols) was added to the pale pink solution. Then, the reaction was heated to 50°C in an oil bath and stirred for 22 h. After which time, the color of the solution changed from pale pink to pale yellow. The solution was concentrated to 5 mL prior to purification by precipitation in hexane. The product was filtered and dried under *vacuo* overnight to obtain an off-white powder. ^1H NMR showed ill-defined resonances. However, the resonances were observed at 7.0 and 3.0 ppm. $^{19}\text{F}\{^1\text{H}\}$ NMR (376.5 MHz, CDCl_3): δ -164.4 ppm (ring residue), δ -165.4 ppm (ring residue), δ -170.4 ppm (ring residue); degree of functionalization: 50% (calcd. from $^{19}\text{F}\{^1\text{H}\}$ NMR integration of the crude product); IR (ATR): 1780 (m), 1689 (m), 1580 (m), 1518 (s), 1435 (m), 994 (m), 752 (m).

3.2.2.4 Attempt to Synthesis of Single-chain Nanoparticles of poly(PFPA)

The modified poly(PFPA) (12.6 mg, 0.00050 mmols) was dissolved in THF with a concentration of 1mg/1mL. A solution of **2** (19.1 mg, 0.028 mmols) in THF was then added to the solution of polymer. While the solution was stirring, NEt_3 (7.3 μL) was added dropwise. The reaction was left stirring for 2 h and then purified via a dialysis method using THF and DCM over three days period. The product was dried under *vacuo*. $^{31}\text{P}\{^1\text{H}\}$ NMR (161.9 MHz, CDCl_3): δ 27.2 ppm.

Chapter 4

Conclusion

Single chain nanoparticles were successfully synthesized via the complexation method between modified poly(PFPA) with 2-aminothiophenol and (dppf)NiCl₂ precursor with a use of triethylamine as a base. ³¹P{¹H} NMR were used to detect the chemical changes which showed the nickel-thiolate bond and nickel-thiolate bridging oligomer. The formation of the SCNPs was also investigated by UV-Visible spectroscopy. Size of obtained nanoparticles were characterised by TEM and DLS indicating diameters of approximately 30-50 nm and 35 nm, respectively. Moreover, the SCNPs could be aggregated with their diameters of 700-2000 nm and 708 nm analyzed by TEM and DLS, respectively.

The homogeneous analogues synthesized to compare the structural properties and catalytic activity, were prepared from the nickel complex precursor ((dppf)NiCl₂), which was made up from 1,1'-Bis(diphenylphosphenyl)ferrocene and nickel chloride hexahydrate (NiCl₂·6H₂O). Compound **3** was synthesized with the nickel precursor and 1,2-benzenedithiol. The product of **3** was obtained 43% yield. Compound **4** was synthesized with the same procedure and thiophenol. The crude product was detected 4 signals of both monomeric and oligomeric form by ³¹P{¹H} NMR. These results could lead to equilibrium of **4** with its oligomeric sulfide bridging complexes.

The preliminary catalytic activity test of **3** investigated by cyclic voltammetry showed the good response to hydrogen evolution.

The SCNPs will be modified to prove its water solubility to perform as a catalyst for hydrogen production by converting proton in aqueous environment along with the catalytic activity of SCNPs will be investigated in the further study.

References

1. Johnston, B.; Mayo, M. C.; Khare, A., Hydrogen: the energy source for the 21st century. *Technovation* 2005, 25 (6), 569-585.
2. Wilberforce, T.; El-Hassan, Z.; Khatib, F. N.; Al Makky, A.; Baroutaji, A.; Carton, J. G.; Olabi, A. G., Developments of electric cars and fuel cell hydrogen electric cars. *International Journal of Hydrogen Energy* 2017, 42 (40), 25695-25734.
3. Carmo, M.; Fritz, D. L.; Mergel, J.; Stolten, D., A comprehensive review on PEM water electrolysis. *International Journal of Hydrogen Energy* 2013, 38 (12), 4901-4934.
4. Kim, C.-H.; Han, J.-Y.; Kim, S.; Lee, B.; Lim, H.; Lee, K.-Y.; Ryi, S.-K., Hydrogen production by steam methane reforming in a membrane reactor equipped with a Pd composite membrane deposited on a porous stainless steel. *International Journal of Hydrogen Energy* 2018, 43 (15), 7684-7692.
5. Mondal, B.; Dey, A., Development of air-stable hydrogen evolution catalysts. *Chemistry Communications* 2017, 53 (55), 7707-7715.
6. Hu, P.; Diskin-Posner, Y.; Ben-David, Y.; Milstein, D., Reusable Homogeneous Catalytic System for Hydrogen Production from Methanol and Water. *ACS Catalysis* 2014, 4 (8), 2649-2652.
7. Gan, L.; Groy, T. L.; Tarakeshwar, P.; Mazinani, S. K.; Shearer, J.; Mujica, V.; Jones, A. K., A nickel phosphine complex as a fast and efficient hydrogen production catalyst. *Journal of the American Chemical Society* 2015, 137 (3), 1109-15.
8. Richards, D. A.; Maruani, A.; Chudasama, V., Antibody fragments as nanoparticle targeting ligands: a step in the right direction. *Chemical Science* 2017, 8 (1), 63-77.
9. Mavila, S.; Diesendruck, C. E.; Linde, S.; Amir, L.; Shikler, R.; Lemcoff, N. G., Polycyclooctadiene complexes of rhodium(I): direct access to organometallic nanoparticles. *Angewandte Chemie International Edition in English* 2013, 52 (22), 5767-70.
10. Mavila, S.; Rozenberg, I.; Lemcoff, N. G., A general approach to mono- and bimetallic organometallic nanoparticles. *Chemical Science* 2014, 5 (11), 4196-4203.
11. Berkovich, I.; Mavila, S.; Iliashevsky, O.; Kozuch, S.; Lemcoff, N. G., Single-chain polybutadiene organometallic nanoparticles: an experimental and theoretical study. *Chemical Science* 2016, 7 (3), 1773-1778.

12. Knofel, N. D.; Rothfuss, H.; Willenbacher, J.; Barner-Kowollik, C.; Roesky, P. W., Platinum(II)-Crosslinked Single-Chain Nanoparticles: An Approach towards Recyclable Homogeneous Catalysts. *Angewandte Chemie International Edition in English* 2017, 56 (18), 4950-4954.
13. Zhang, J.; Tanaka, J.; Gurnani, P.; Wilson, P.; Hartlieb, M.; Perrier, S., Self-assembly and disassembly of stimuli responsive tadpole-like single chain nanoparticles using a switchable hydrophilic/hydrophobic boronic acid cross-linker. *Polymer Chemistry* 2017, 8 (28), 4079-4087.
14. Zhu, B.; Sun, S.; Wang, Y.; Deng, S.; Qian, G.; Wang, M.; Hu, A., Preparation of carbon nanodots from single chain polymeric nanoparticles and theoretical investigation of the photoluminescence mechanism. *Journal of Materials Chemistry C* 2013, 1 (3), 580-586.
15. Perez-Baena, I.; Loinaz, I.; Padro, D.; García, I.; Grande, H. J.; Odriozola, I., Single-chain polyacrylic nanoparticles with multiple Gd(iii) centres as potential MRI contrast agents. *Journal of Materials Chemistry* 2010, 20 (33), 6916.
16. Qian, G.; Zhu, B.; Wang, Y.; Deng, S.; Hu, A., Size-tunable polymeric nanoreactors for one-pot synthesis and encapsulation of quantum dots. *Macromol Rapid Commun* 2012, 33 (16), 1393-8.
17. Gillissen, M. A. J.; Voets, I. K.; Meijer, E. W.; Palmans, A. R. A., Single chain polymeric nanoparticles as compartmentalised sensors for metal ions. *Polymer Chemistry* 2012, 3 (11), 3166.
18. Sanchez-Sanchez, A.; Arbe, A.; Colmenero, J.; Pomposo, J. A., Metallo-Folded Single-Chain Nanoparticles with Catalytic Selectivity. *ACS Macro Letters* 2014, 3 (5), 439-443.
19. Martínez-Prieto, L. M.; Carencó, S.; Wu, C. H.; Bonnefille, E.; Axnanda, S.; Liu, Z.; Fazzini, P. F.; Philippot, K.; Salmeron, M.; Chaudret, B., Organometallic Ruthenium Nanoparticles as Model Catalysts for CO Hydrogenation: A Nuclear Magnetic Resonance and Ambient-Pressure X-ray Photoelectron Spectroscopy Study. *ACS Catalysis* 2014, 4 (9), 3160-3168.
20. Thanneeru, S.; Duay, S. S.; Jin, L.; Fu, Y.; Angeles-Boza, A. M.; He, J., Single Chain Polymeric Nanoparticles to Promote Selective Hydroxylation Reactions of Phenol Catalyzed by Copper. *ACS Macro Letters* 2017, 6 (7), 652-656.
21. Hanlon, A. M.; Lyon, C. K.; Berda, E. B., What Is Next in Single-Chain Nanoparticles? *Macromolecules* 2015, 49 (1), 2-14.

22. Rubio-Cervilla, J.; Gonzalez, E.; Pomposo, J. A., Advances in Single-Chain Nanoparticles for Catalysis Applications. *Nanomaterials* 2017, 7 (10).
23. Huo, M.; Wang, N.; Fang, T.; Sun, M.; Wei, Y.; Yuan, J., Single-chain polymer nanoparticles: Mimic the proteins. *Polymer* 2015, 66, A11-A21.
24. Liu, Y.; Pujals, S.; Stals, P. J. M.; Paulohrl, T.; Presolski, S. I.; Meijer, E. W.; Albertazzi, L.; Palmans, A. R. A., Catalytically Active Single-Chain Polymeric Nanoparticles: Exploring Their Functions in Complex Biological Media. *Journal of the American Chemical Society* 2018, 140 (9), 3423-3433.
25. Wulff, G.; Chong, B. O.; Kolb, U., Soluble single-molecule nanogels of controlled structure as a matrix for efficient artificial enzymes. *Angewandte Chemie International Edition in English* 2006, 45 (18), 2955-8.
26. Huerta, E.; Stals, P. J.; Meijer, E. W.; Palmans, A. R., Consequences of folding a water-soluble polymer around an organocatalyst. *Angewandte Chemie International Edition in English* 2013, 52 (10), 2906-10.
27. Willenbacher, J.; Altintas, O.; Trouillet, V.; Knöfel, N.; Monteiro, M. J.; Roesky, P. W.; Barner-Kowollik, C., Pd-complex driven formation of single-chain nanoparticles. *Polymer Chemistry* 2015, 6 (24), 4358-4365.
28. Bai, Y.; Feng, X.; Xing, H.; Xu, Y.; Kim, B. K.; Baig, N.; Zhou, T.; Gewirth, A. A.; Lu, Y.; Oldfield, E.; Zimmerman, S. C., A Highly Efficient Single-Chain Metal-Organic Nanoparticle Catalyst for Alkyne-Azide "Click" Reactions in Water and in Cells. *Journal of the American Chemical Society* 2016, 138 (35), 11077-80.
29. Thanneeru, S.; Nganga, J. K.; Amin, A. S.; Liu, B.; Jin, L.; Angeles-Boza, A. M.; He, J., "Enzymatic" Photoreduction of Carbon Dioxide using Polymeric Metallofoldamers Containing Nickel-Thiolate Cofactors. *ChemCatChem* 2017, 9 (7), 1157-1162.
30. Ajo, U. C. a. D., Heteropolymetallic complexes of 1,1'-bis(diphenylphosphino) ferrocene (dppf). II. Crystal structure of dppf and NiCl₂(dppf). *Journal of Crystallographic and Spectroscopic Research* 1988, 18 (5), 583-590.
31. Thomas B. Rauchfuss, J. S. S. a. D. M. R., Synthesis and Chemistry of New Nickel, Palladium and Platinum Complexes of 1,2-Ethanedithiol, 1,3-Propanedithiol, 1,4-Butanedithiol, 1,4,8-Trithianonane and 1,4,8,11-Tetrathiaundecane. *Inorganic Chemistry* 1976, 15 (9), 2096-2101.

32. Liu, Y.; Pauloehrl, T.; Presolski, S. I.; Albertazzi, L.; Palmans, A. R.; Meijer, E. W., Modular Synthetic Platform for the Construction of Functional Single-Chain Polymeric Nanoparticles: From Aqueous Catalysis to Photosensitization. *Journal of the American Chemical Society* 2015, 137 (40), 13096-105.
33. Jochum, F. D.; Theato, P., Temperature- and Light-Responsive Polyacrylamides Prepared by a Double Polymer Analogous Reaction of Activated Ester Polymers. *Macromolecules* 2009, 42 (16), 5941-5945.
34. Gao, X.; Yu, B.; Mei, Q.; Yang, Z.; Zhao, Y.; Zhang, H.; Hao, L.; Liu, Z., Atmospheric CO₂ promoted synthesis of N-containing heterocycles over B(C₆F₅)₃ catalyst. *New Journal of Chemistry* 2016, 40 (10), 8282-8287.
35. Gupta, P.; Paul, S., Amorphous carbon-silica composites bearing sulfonic acid as solid acid catalysts for the chemoselective protection of aldehydes as 1,1-diacetates and for N-, O- and S-acylations. *Green Chemistry* 2011, 13 (9), 2365.
36. Kovacic, J. E., The C=N stretching frequency in the infrared spectra of Schiff's base complexes-I. Copper complexes of salicylidene anilines. *Spectrochimica Acta* 1967, 23A, 183-187.
37. Engl, O. D.; Saadi, J.; Cosimi, E.; Wennemers, H., Synthesis of Monothiomalonates - Versatile Thioester Enolate Equivalents for C-C Bond Formations. *Helvetica Chimica Acta* 2017, 100 (11), e1700196.
38. S., P., Preparation and structures of 1'-(diphenylphosphino)ferrocenecarboxaldehyde and {1'-(diphenylphosphino)ferrocenyl}methanol. *Inorganic Chemistry Communications* 2001, 4, 682-687.
39. M., L. L., Bidentate aryldichalcogenide complexes of (diphosphino)ferrocene]palladium(II) and [(diphosphino)ferrocene]platinum(II). Synthesis, molecular structures and electrochemistry. *Polyhedron* 2001, 20, 3189-3200.
40. Wang, Q.; Marr, A. C.; Blake, A. J.; Wilson, C.; Schröder, M., Formation of nickel-thiolate aggregates via reaction with CH₂Cl₂. *Chemical Communication* 2003, (22), 2776-2777.
41. A., G., Electrochemical and ESR Studies of the Redox Reactions of Nickel(II), Palladium(II), and Platinum(II) Complexes of 1,2-Diphenyl- 1,2-ethenedithiolate(2-)-S,S'. *Inorganic Chemistry* 1983, 22, 1208-1213.

42. Usón, M. A.; Llanos, J. M., Synthesis of Group 10 polyfluorothiolate mono- and binuclear complexes. Crystal structures of $[\text{Ni}(\text{SC}_6\text{HF}_4)_2(\text{dppe})]$, $[(\text{dppe})\text{Ni}(\mu\text{-SC}_6\text{HF}_4)_2\text{Pd}(\text{C}_6\text{F}_5)_2]$ and $[(\text{dppe})\text{Ni}(\mu\text{-SC}_6\text{F}_5)_2\text{Pd}(\text{C}_6\text{F}_5)_2]$. *Journal of Organometallic Chemistry* 2002, 663 (1-2), 98-107.
43. Decker, C.; Henderson, W.; Nicholson, B. K., Platinum(II), palladium(II), nickel(II), and gold(I) complexes of the “electrospray-friendly” thiolate ligands 4-SC₅H₄N– and 4-SC₆H₄OMe–. *Journal of Coordination Chemistry* 2010, 63 (17), 2965-2975.
44. Owen, S. C.; Chan, D. P. Y.; Shoichet, M. S., Polymeric micelle stability. *Nano Today* 2012, 7 (1), 53-65.



Vita

Mr. Thongpon Meethong was born on March 2nd, 1996 in Chonburi, Thailand. He got a high school diploma from Saint Gabriel's College in Mathematics-Science program, Bangkok in 2013. He started as a bachelor's Degree student in Department of Chemistry, Faculty of Science, Chulalongkorn University in academic year 2014. His current address is 110/174 Krissadanakhon city 26 village, Nakhonchaisri, Nakhonpathom 73120.

